人類腦神經膠質瘤 U138MG 細胞株經輻射照射後之時程性基因表現

Microarray Analysis of Temporal Gene Responses to Ionizing Radiation on U138 Glioma Cell Line

研究生 ： 李威德 **(Wei-Te Lee)**

指導老師 ： 吳國海 **(Frank Q.H. Ngo)**

國立陽明大學

放射醫學科學研究所

碩士論文

National Yang-Ming University

Institute of Radiological Sciences

Master Thesis

中華民國九十三年八月

August 2004

Contents

中文摘要

人類腦神經膠質瘤在臨床分級上屬惡性度最高的第四級，目前標準之治療程序為手術後合併放射線或化學治療，然而其成效並不顯著。使得腦神經膠質瘤病人預後較差的其中一個原因可能與其腫瘤細胞本身具有相當的輻射耐受性(radio-resistence)有關。本實驗旨在研究 p53 基因突變之腦瘤細胞株 U138MG 之輻射敏感度並藉由基因表現來了解相關之分子機制。我們利用高密度之寡核酸(oligo)微陣列分析來追蹤 U138MG 細胞經 1%致死劑量(10 格雷加馬射線)照射下其時程性基因表現，並輔以適當之資料過濾(filtering)以及統計運算以篩選出具有差異性表現之基因群，且結合生物統計之相關資訊以找出具有特殊生物意義之功能性基因群。細胞對加馬射線之存活曲線則以群落形成測試法(colony-forming assay)測得。此外，為了研究受輻射照射後之細胞其細胞週期的改變及細胞凋亡(apoptosis)反應，我們分別在照射後不同時間點收取細胞進行細胞週期的分析以及 DNA 段裂(DNA ladder)的量測。結果顯示，細胞經 10 格雷加馬輻射照射後，其細胞週期會延滯在 G2/M 期，且在照射後 36 小時達到最大量，約有 80%的細胞停留在 G2/M 期，同時在照射後四天內皆沒有量測到 DNA 段裂的現象。在微陣列基因表現分析中，集群(clustering)分析可以將差異性表現的基因主要分為兩大類，其中一類是屬於早期表現(early responded)的基因群，其內含之基因大多與調控細胞週期有關，另一類則屬於晚期表現(late responded)的基因群，其表現量之改變則涉及許多生物功能。其中，第一類基因與實驗中 G2/M 細胞週期檢查點之引發相吻合。值得注意的是，基因表現分析顯示在照射後 6 到 12 小時有一組與調控細胞分裂有關之

基因群呈現明顯之抑制。綜合上述，我們推測 U138MG 細胞由於 p53 蛋白之突變而缺乏細胞凋亡之現象，使得輻射引起之死亡主要來自於輻射引起之增殖死亡(mitotic death)，並進而導致細胞無法在長時間之 G2 期阻滯中進行損傷之修補。此推測可由基因表現分析之結果得到相關之證實。

Abstract

Being rated as Grade IV, glioblastoma multiforme (GBM) is the most aggressive pathological form of glioma in the central nervous system. The standard way of treating a GBM patient is through surgical resection followed by radio- and/or chemotherapy. However, the median life expectancy after the therapies remains poor. One of the possible causes of the poor prognostic property of GBM can be associated with the relative radio-resistance of the tumor cells. In this thesis, we have employed a U138MG glioma cell line which contains mutated p53 and attempted to understand the radiosensitivity of this cell line via global transcriptional activities. Temporal global gene expression profiling were traced using high-density oligo microarrays, following 10Gy gamma-irradiation, a dose that reduced colony survival of U138 to about 1%. Appropriate filtering and statistical methods were used to search for significantly altered genes and genes of functional interest were identified using bioinformatics sources. Colony-forming assay was used to obtain the survival response curve to gamma irradiation. To investigate the cell-cycle perturbations and apoptotic events as induced by irradiation, we harvested cells at different incubation times post irradiation (PI) for DNA content analysis and DNA laddering assay, respectively. The data indicated that while there was an extended G2/M arrest of the irradiated cells with a maximum 80% accumulation at 36hrs after 10Gy irradiation, there was no evidence of DNA laddering detectable up to 4 days PI. For the microarray gene expression data, our cluster demonstrated that genes could be divided into two categories: one is the early responded genes, of which most of these genes are related to regulation of cell cycle; the other is the late responded genes, most of which

are involved in regulation of multiple biological functions. The changes of expression levels of the former appeared to be consistent with the G2/M checkpoint activities. Interestingly, the data revealed that a group of genes whose functions are in the control of mitotic events were down-regulated from 6-12hrs PI. In conclusion, we speculate that the lack of apoptotic events may be explained by the dysfunction of the p53 in U138MG, whereas the radiation-induced cell death would have to come from a catastrophe of mitotic death, following a failure of an attempt to repair damage in an extensive period of G2 arrest. Such a mechanism of radiation-induced cell death would be supported by the results of our gene expression analysis.

I. INTRODUCTION

Glioblastoma multiforme

Astrocytic tumors are divided into two basic categories: circumscribed (grade I) or diffuse (grades II-IV), and all diffuse astrocytomas tend to progress to grade IV astrocytoma. Glioblastoma multiforme (GBM), which is synonymous with grade IV astrocytoma and the most common type of brain tumor, is considered to be one of the most malignant human neoplasms, and is also the most deadly[1]. GBMs are characterized by marked neo-vascularity, increased mitosis, greater degree of cellularity and nuclear pleomorphism, and microscopic evidence of necrosis. It arises either through an anaplastic progression from a lower-grade astrocytoma or *de novo*, without evidence of an antecedent lesion.

Modern, effective treatment for GBM includes surgery, which is to remove the maximum volume of tumor, followed by radio- and/or chemotherapy. The median survival of patients with malignant gliomas without treatment is 14 weeks; by surgical resection alone, 20 weeks; by surgery and radiation, 36 weeks; and by the addition of chemotherapy, 40-50 weeks[2,3,4,5]. Despite the advances in microneurosurgery, developments in the technology and techniques of radiation administration, advances in imaging, and introduction of novel chemotherapeutic agents, the median life expectancy for GBM patients remains poor, and only 5% of patients or fewer will be alive within five years after initial diagnosis. So far, external beam radiation remains the sole therapy that demonstrably increases the survival of patients with GBM, and yet it still provides only modest benefit[6]. However, malignant glioma cells are remarkably resistant to ionizing radiation, and the association of a significant portion of these cells with

necrotic and hypoxic tissues further increases their resistance[7].

Oncogenic mutations on TP53

Neoplastic transformation appears to be a multi-step process in which the normal controls of cell proliferation and cell-cell interaction are lost, thus transforming a normal cell into a cancer cell[8]. The process of carcinogenesis involves the gain of oncogene activity and the lost of tumor suppressor gene function. A key tumor suppressor gene often lost is p53, whose activation can induce temporary cell cycle arrest, irreversible growth arrest, promoting DNA repair, or activating apoptosis in response to potentially oncogenic cellular stress[9,10]. The mutation of *p53* gene is involved in the early stages of astrocytoma tumorigenesis[11]. For instance, *p53* mutations and allelic loss of chromosome 17p are observed in approximately one-third of all three grades of adult astrocytomas. Moreover, high grade astrocytomas with homogeneous *p53* mutations evolve clonally from subpopulations of similarly mutated cells present in initially low grade tumors[12], suggesting that inactivation of *p53* is important in the formation of neoplastic transformation and in facilitating it malignant progression.

The *p53* tumor suppressor gene is mutated in over 50% of human cancers, and most of these mutations are missense, which results in full-length, but mutant, proteins[13,14]. Extensive data suggest that many missense mutations in *p53* abolish it ability to bind specific DNA sequences and can inhibit the function of the wild-type protein in a dominant-negative manner[15]. For example, one important feature of the oncogenic activity of p53 mutants is their ability to interfere with p53-denpendent apoptosis by a dominant negative mechanism. On the other hand, a p53-independent

apoptosis has been reported, by a yet unknown mechanism that may involve transactivation and/or participation of other members of p53 family[16,17].

Responding to DNA damage

DNA damage may be caused by the cell's own error-prone internal machinery, the metabolic environment or by external physical and/or chemical agents (e.g. radiation or carcinogens). The inability to repair DNA damage properly in cells leads to cell death or enhanced oncogenic transformation. Cells respond to DNA damage by activating a complex DNA-damage-response pathway, which includes cell-cycle arrest, the transcriptional activation of a subset of genes, the post-transcriptional regulation of associated proteins, and, under some situations, triggering cell death[18,19,20]. For instance, checkpoints respond to DNA damage by arresting the cell cycle which can provide time for DNA repair and by inducing transcription of genes that facilitate the process of repair.

In mammalian cells, three important proteins control the DNA damage checkpoints, mutated in ataxia telangiectasia (ATM), Chk2, and p53[21]. In general, the kinase activity of ATM is enhanced after DNA damage and activation of ATM kinase is capable of phosphorylating p53. Phosporylation of p53 at Ser15 by ATM correlates both the accumulation of total p53 protein and the ability of p53 to transactivate downstream target genes, such as *p21* and *YWHAD*, through transcription-dependent manner[22]. Activated p21 can inhibit phosphorylation and activation of G1-specific cyclin/cdk complexes, and susequently arrests cells at G1-phase[23]. And also, activation of YWHAD enhances negative regulation of Cdc25C and prevents the activation of Cdc2-cyclin B1 complexes, thereby prevents cells from

entering into mitosis[24,25]. Besides, p53 also induces apoptosis while cell-cycle checkpoints were activated. Many p53-inducible genes include *BAX*, *TNFRSF6* and *TNFRSF10B*, which are all classical members of the core apoptosis pathways, and activation of these proteins may lead to cell death[18,26,27]. In this case, p53 provides a possibility to cells to make decision between life and death[28]. However, in contrast with cells bearing wild-type *p53*, cells with defective *p53* are unable to arrest cell cycle at G1 in response to ionizing irradiation and show reduced apoptosis[16,29]. For this reason, cells with mutated p53 gene are resistant to radiation due to contributions of loss of p53-dependent cell-cycle checkpoint and insufficient to induce apoptosis.

Global gene expression analysis by DNA microarray

Among the techniques of functional genomics, microarray provides a good appliance for the study of complex biological systems with applications to life sciences and molecular medicine. This novel and powerful gene expression profiling technique permits the analysis of the expression levels of thousands of genes simultaneously in a single experiment, and sufficiently generate a vast amount of data that may lead to a better understanding of the regulatory events involved in the transcription level of biological systems[30,31].

Microarrays are usually made by deposition of cDNA or oligonucleotide molecules onto spots on a solid support like a coated glass surface or on filter-based supports, such as charged nylon or nitrocellulose. The design of the glass slides makes it possible (i) to provide an optimized environment for taking up hybridization reactions between arrayed probes and the target genes from samples and (ii) to use fluorescent dyes for detection and allow

focusing by laser scanning confocal microscopy. Two main procedures have been used to produce cDNA or oligo chips: photolithography[32] as developed by Affymetrix Inc. and mechanical gridding methods[33,34], which are based on ink-jet (Agilent Technologies) or physical spotting (Amersham Biosciences) of the materials using pins manufactured with very high precision . For mRNA samples, the two samples or targets are reversely transcribed into cDNA and labeled using different fluorescent dyes. When performing experiments, targets from two different conditions were mixed in equal properties and hybridized to the arrayed probes. After this competitive hybridization, the slides then are imaged using a scanner and the intensities of each fluorescence channel can be determined.

Microarray can be used to identify novel networks of gene activities and to investigate the expression patterns or profiles. Many articles have reported the use of microarrays for studying human diseases and their associated variations and understanding the regulatory mechanisms in molecular biology[35,36,37]. For these purposes, samples from clinical tissues, human cell lines, and RNA from animal model systems have been used extensively in microarray analysis.

Study Purpose

Malignant glioma cells are remarkably resistant to ionizing radiation, and the association of more than one-third of these cells with mutations on *p53* tumor suppressor gene may be one factor that would confer their resistance to radiation treatment and chemotherapy agents[38]. However, radiation treatment on glioma patients remains the sole agent that evidently can prolong life of patients. Therefore, understanding of radiation effect on

glioma is important in developing more effective therapeutic approaches against the devastating neoplasm.

Here, U138MG cell line was introduced as the object of our *in vitro* study. The glioblastoma cell line U138MG was proved to have a mutated *p53* gene, from Arg to Gln at codon 213, and produced a loss-of-function p53 protein[39]. In a previous study form our laboratory, the effects on cell-cycle distribution of irradiated U138 cells were investigated, and the gene expression profiles were evaluated using cDNA microarray technology[40]. Microarray analyses revealed changes in the expression of a number of genes, like CDC2, CDC25 and CCNB1, were related to the regulation of cell-cycle progression. A TP53-independent pathway in regulating cell-cycle progression was also proposed. In this study, a temporal expression profile induced by gamma-irradiation was determined, using oligonucleotide microarray, and advanced data analysis methods were performed. In addition to the study of cell cycle perturbation as induced by radiation, we also intended to investigate the transcriptional regulations on other biological responses which include apoptosis and other aspects. In doing so, we attempted to explain the mechanisms with which U138MG glioblastoma cells are killed by ionizing irradiation. Understanding of these events may not only enhance our knowledge on the mechanisms of a p53-mutated glioma cells responding to ionizing irradiation, but also provide insights for the relationships between radiation-induced cell cycle checkpoints and cell death.

II. MATERIALS AND METHODS

Cell Culture. The glioblastoma cell line U138MG was obtained from the American Type Culture Collection (ATCC). U138 cells contains a mutated p53 (from Arg to Gln at codon 213) gene which produces a non-function mutated-p53 (mt-p53) protein. Cells were grown in Minimum Essential Medium (Gibco) supplemented with 10% FBS and 1% antibiotic-antimycotic (Gibco). Cultures were maintained at 37^{o}C in a humidified atmosphere containing 5% CO_2.

Growth Curve. From a growth curve, the population doubling time and saturation density can be determined. Briefly, 1×10^4 cells were suspended in 5ml of medium and seeded into a 60-mm dish. Cultures were incubated and triplicate plates were counted every 48 hours. By plotting the results of cell number and time on a log-linear scale, population-doubling time can be determined by identifying a cell number along the exponential phase of the curve.

Radiation Treatment. Radiation treatments were performed with a ^{60}Co Theraton irradiator (Atomic Energy of Canada, Limited). The dose rate was 29-32 cGy/min. One third of medium were refreshed at the day before treatment and irradiated within 24 hours. After treatment, cells were incubated and harvested at selected time points.

Clonogenic Suvival Assay. For determination of colony-forming ability following irradiation, cells were plated in 60-mm dishes. After 10-day

incubation at 37^{o}C, colonies were stained with 0.5% crystal violet (Sigma) and the numbers of colonies of 50 or more cells were counted. Surviving fraction values were calculated and normalized with plating efficiency (PE) obtained from non-irradiated cells.

DNA Content Analysis. For flow cytometry analysis, cells were harvested with 0.25% trypsin-EDTA at each time points, fixed with 70% ethanol for at least 4 hr and stored at -20^{o}C for up to 3 days. Before staining, the fixative was thoroughly removed by centrifugation, then cells were resuspended in 200 μl of phosphate-citrate buffer, consisting of 192 parts of 0.2M Na_2HPO_4 and 8 parts of 0.1M citric acid (pH 7.8), at room temperature, for at least 30 min[41]. After centrifugation, the samples were treated with 1 mg/ml RNase A and stained with 400 μg/ml propidium iodide for 30 min at 37^{o}C incubation. Samples were analyzed by using a FACSCalibur flow cytometer (Becton Dickinson) with CELLQUEST software (distributed by Becton Dickinson). At least 10,000 cells were collected. Cell cycle distribution was determined using ModFit (Verity Software House) software. Experiments were repeated at least three times.

DNA Laddering Assay. Apoptotic DNA Ladder Kit (Roche) was used to detect fragmented DNA followed the manufacturer's instruction. Briefly, 2×10^6 cell were harvested, centrifuged and the medium was removed. After lyses of cells in binding buffer (6M guanidine-HCl, 10mM urea, 10mM Tris-HCl and 20% Triton X-100 (v/v) pH 4.4), the lysate is applied to a filter tube with glass fiber fleece and passed through the filter by centrifugation. During this procedure, nucleic acids bind specifically to the surface of glass

fibers in the presence of chaotropic salts. Residual impurities are removed by a wash step and subsequently DNA is eluted in elution buffer (10mM Tris, pH 8.5). For each well, either 3 μg of purified DNA or 15 μl of positive control DNA was mixed with loading buffer, then, loaded onto 1.5% agarose gel and performed at 100V for 35 min. The positive control DNA, which provided by this kit, was isolated from U937 cells treated with 4 μg/ml camptothecin for 3 hours, usually resulting in about 30% apoptotic cells. The 100 bp DNA Ladder (Invitrogen) used here as markers consists of 15 blunt-ended fragments between 100 and 1500 bp in multiples of 100 bp and an additional fragment at 2072 bp.

Total RNA Isolation. The total RNA was isolated from about 5×10^6 cells using RNeasy Mini kit (QIAGEN) according to the manufacturer's instructions. In brief, cells are first lysed and homogenized in the presence of a highly denaturing guanidine isothiocyanate-containing buffer, which immediately inactivates RNases to ensure isolation of intact RNA. Ethanol is then added to provide appropriate binding conditions, and applied to RNeasy mini column where the total RNA binds to the membrane and contaminants are washed away. Finally, total RNA is eluted in 80 μl RNase-free water and stored at -80^{o}C until use. The RNA concentration and it purity was determined using spectrophotometer, and the quality of total RNA was checked by measuring the 28S/18S ribosomal RNA ratio.

Fluorescent cRNA Generation. Synthesis and labeling of cRNA was carried out using the Low RNA Input Fluorescent Linear Amplification Kit (Agilent Technologies) according to the manufacturer's instructions. Two μg

of total RNA was used in each of the labeling reactions, then is amplified and converted to either fluorescently Cy3- or Cy5-labeled cRNA. In brief, a primer, which contains poly dT and a T7 polymerase promoter, is used to anneal to the poly A^+ RNA, and a reverse transcriptase (MMLV-RT) is then added to synthesize the first and second strands of cDNA. Thus, double-stranded cDNA has been synthesized. Finally, cRNA is synthesized using T7 RNA polymerase, which simultaneously incorporates Cy3- or Cy5-labeled CTP. Each Cy3- and Cy5-labeled cRNA was purified using RNeasy Mini Kit (QIAGEN). The amount of amplified cRNA was determined using spectrophotometer.

Oligonucleotide Microarray. We used the oligonucleotide microarray produced by Agilent Technologies, Human 1A Oligo Microarray (G4110B), that contains over 22,000 unique 60-mer oligos representing over 18,000 unique human genes sourced from Incyte's Genomics Foundation Database. The samples were paired as described. The hybridization procedure was followed the manufacturer's specifications. Briefly, both 0.75 μg of Cy3- and Cy5-labeled cRNA were mixed with control targets and fragmentation buffer. Mixtures were incubated at 60^{o}C for 30 min. In this step, cRNA strands were fragmented into short strands whose lengths are optimal for binding to probes on the chips. In order to terminate the fragmentation reaction, the hybridization buffer was added. Reactions were performed using hybridization chambers (G2531A) in the hybridization oven, at 60^{o}C for 17 hours. Finally, hybridized slides were washed using wash solution 1 (6X SSC, 0.005% Triton X-102) for 10 min and wash solution 2 (0.1X SSC, 0.005% Triton X-102) for 5 min. Cy3 and Cy5 fluorescences were scanned

using Agilent's dual-laser Microarray Scanner (G2565BA), and images were analyzed using Feature Extraction 7.1 (G2567AA).

Data Analysis. Data generated from Feature Extraction were analyzed using GeneSpring^{TM} 6.1.1 (Silicon Genetics). The dye-swap data were normalized and averaged with Lowess method. For each gene, the significance between repeat experiments was calculated by the Cross-Gene Error Model built within GeneSpring. Genes were considered differentially expressed only when they passed the following criteria. First, only those genes that were flagged as "IsPosAndSignif" by Feature Extraction software in both Cy3 and Cy5 channels, which means the extracted signal is greater than and significant compared to the background signal, were considered good quality data and were used for further analysis. Second, those genes with normalized ratio $\geqq$ 1.35 or $\leqq$ 0.74 and t-test p-value lesser than 0.05 were regarded as expressed genes. Then, the genes, which passed the criteria and overlapped from two independent microarray experiments, were identified as differentially expressed genes (DEGenes).

Functional classification was performed on Onto-Express (OE)[42] and GOTree Machine (GOTM)[43], which both are web-based platforms, to automatically translate a list of genes into functional profiles. The DEGenes list was used in functional classification and the results from both OE and GOTM were integrated and divided into seven groups manually according to their biological functions. To make the orderly features in the data more apparent, we used a hierachical clustering algorithm in data analysis. The object of the clustering was to group genes whose expression ratio varied with time PI in a similar manner. Clustering was performed using DEGenes.

In this case each gene has ten ratio values corresponding to five time points each in two experiments. The clustering algorithm measured the distance between each gene and the similarity between each sample using standard and pearson correlation, respectively.

Real-Time RT-PCR. In order to validate the data obtained from microarray, the quantitative RT-PCR was performed using the same RNA source as that used in the microarray experiments. cDNA synthesis and SYBR Green I RT-PCR were carried out according to the manufacturer's instructions. In brief, first strand cDNA was synthesized using SuperScript II Reverse Transcriptase (Invitrogen). The final concentration for the cDNA reaction in a 40 μl volume was 2 μg total RNA, 2 μl $Oligo(dT)_{12-18}$ (500 μg/ml) and 2 μl 10mM dNTP mix (Amersham Biosciences), 8 μl 5X First-Strand Buffer, 4 μl 0.1M DTT, 2 μl RNasin Ribonuclease Inhibitor (Promega) and 2 μl SuperScript II RT. The synthesized cDNA was then purified using QIAquick PCR Purification Kit (QIAGEN), eluted with 50 μl Buffer EB (10mM Tris-Cl, pH 8.5) and stored at -20^{o}C.

Real-time PCR amplification mixtures (30 μl) contained 1 μl of cDNA eluate, 15 μl 2X SYBR Green I Master Mix buffer (Applied Biosystems) and 200nM forward and reverse primer. The primers for PCR reactions were queried from two primer databases, Quantitative PCR Primer Database (distributed from NCI) and methPrimerDB (distributed from Centre for Medical Genetics, Ghent University). Reactions were run on an ABI PRISM 7000 Sequence Detection System (Applied Biosystems). The cycling conditions comprised 10 min polymerase activation at 95^{o}C, 40 cycles at 95^{o}C for 15 sec and 60^{o}C for 60 sec. For each gene, we selected a

non-template control (NTC) for each assay was performed in triplicate. Results analyzed with ABI PRISM 7000 SDS Software (version 1.1) were exported as tab-delimited text files and imported into Microsoft Excel for further analysis. The gene expression was determined by using relative quantification method[44,45].

III. RESULTS

Growth kinetics and radiation-induced cell killing

After calculating the increasing population against incubation time, the population-doubling time of U138 cells was estimated to be 39.3 hrs. For determination of the colony-forming ability, cells were irradiated with single doses of gamma-rays using a ^{60}Co irradiator. Controls were shame-irradiated. Figure 1 shows the survival curve of U138MG for gamma irradiation.

Cell cycle perturbation on U138 cells after ionizing radiation

To investigate the effects of gamma-irradiation on the cell-cycle distribution in U138MG cells, FACS analysis was performed on the DNA content of the controlled and 10Gy irradiated cells at various times PI. Figure 2 shows the histogram of DNA content analysis on each time point. Subpopulation of cells contain 2N (G1 phase) and 4N (G2/M phase) DNA were separated into two distinct peaks, and between the two peaks was S phase. The subpopulation before G1 peak was defined as debris which indicated the dead cells or cluster of DNA fragments. The percentage of cells distributed in each phase was calculated with ModFit software. In irradiated cells, the population of G2/M-phase cells increased gradually and reached maximum at 36h, and, at the same time, the population of G1-phase cells decreased initially after irradiation, then increased at 24h, implying that the damaged cells were arrested at G2/M phase after IR and continued for at least 24h. Then some of the arrested cells might be released from G2 arrest and started to enter cell cycle, while the remaining could be further arrested in M phase. The above description is still a speculation since one cannot

distinguish between G2 and M cells on the DNA content alone. However, since even at 72hrs PI, there still considerable proportion of G2/M cells, the data here suggest that the arrested population did not exhibit a full recovery, and probably half of the cells were still retained at G2 phase. Finally, the population of S-phase cells transiently increased at 6 to 12h and the amount of debris increased with time PI, implying the existence of delayed S-phase progression and accumulation of dead cells, respectively.

Detection of DNA laddering

A cell which was triggered to apoptosis is thought to activate a cascade of characteristic molecular events that stepwise lead to its total disintegration. One of the late events is DNA fragmentation[46,47]. In an earlier study[40], Hsiao proposed that following G2/M arrest due to irradiation, U138 cells would undergo apoptotic death. To investigate this possibility, we have performed gel electrophoresis for detection of DNA laddering fragments which would represent activation of apoptosis. After 10Gy irradiation, cells were incubated and harvested at various time points. In these experiments, we found that no evidence of DNA laddering at different duration post-irradiation ranging from 0.5h to 4d. The results are provided in Figure 3. Here, a clear DNA laddering was detected at the column of positive control. On the basis of these results, we propose that the majority of irradiated U138 cells were blocked at G2/M phase for a long time which may even last to 72h or longer, and a portion of cells undergo cell death via some pathways, such as mitotic catastrophe or autophagy, other than apoptosis[48,49]. The following analysis with gene expression data would support the notion that mitotic death would be the dominant events.

Identification of differentially expressed genes

Microarray analysis of temporal response of global gene expression was performed using total RNA from 10Gy gamma-irradiated U138 cells harvested at selected time points PI (0.5, 6, 12, 24, 36 hrs). Their corresponding controls were from non-irradiated cells harvested at 0.5h. The collected cells were stored at -80^{0}C freezer and total RNA were extracted within three days to avoid the degradation of RNA. The quantity and quality of total RNA was measured and evaluated using spectrophotometer and formaldehyde-agarose (FA) gel electrophoresis, respectively. To ensure the reproducibility and accuracy of microarray experiments, and prevent RNA from degradation, it is important to maintain an RNase-free environment during these procedures.

During acquisition of data, the intensities from both Cy3 and Cy5 channels were detected by a dual-laser confocal microscopic scanner and the expression of genes was quantitatively determined by Feature Extraction software. Figure 5 shows the M-A plots, which was used to illustrate intensity-dependant ratio (M) of raw microarray data, and the relative amount of each gene (A)[50]. Here, one can see that the population of genes expressed with lower intensities scattered from zero much more comparing to the population of genes expressed with higher intensities. This may be caused by several possibilities: (a) the design of the probes on chip, (b) the background generated from slides or impurities, (c) the abundance of the RNA targets, (d) the specificity and sensitivity of the scanner, and, other parameters yet to be determined. To reduce or remove this systematic bias, one cam perform a Lowess normalization. Figure 5 also shows the data after Lowess normalization where the noises in the low-intensity region was

much reduced.

Finally, the data from two independent microarray experiments were collected and analyzed using GeneSpring software by procedure described in the Methods section. Through these steps of filtering procedure, we have eventually identified 191 out of 20,173 genes as differentially expressed genes.

Functional classification and clustering

Microarrays allow researchers to screen tens of thousands of genes simultaneously, and generate a staggering amount of data. Typically, the first step is to identify a set of differentially regulated genes, as we have done. However, a major challenge has been to interpret the results of these activities in the context of the observed phenomena. Here, we attempted to understand how cells were responding to irradiation, by first investigating the gene expression data using a Java-based program called Onto-Express (OE)[42,51]. This algorithm uses UniGene accession or cluster identification numbers generated from microarray investigations to search the public databases to return the functional profiles for each gene. OE constructs functional profiles, using Gene Ontology terms, for the following categories: biochemical function, biological process, cellular role, cellular component, molecular function and chromosome location. Another web-based platform for interpreting sets of interesting genes using Gene Ontology hierarchies, GOTree Machine (GOTM), was also used in comparing the results from OE[43]. GOTree Machine can generate a GOTree, a tree-like structure to navigate the Gene Ontology Directed Acyclic Graph for input gene sets. Statistical analysis, which compares the interesting genes and the reference

genes, was also performed in both programs, and the enriched gene numbers can be presented in text format (OE) or DAG view format (GOTM).

The DEGenes list was used in functional classification and the results from both OE and GOTM were integrated and divided into seven groups manually according to their biological functions (Table 1). The functions included cell cycle, apoptosis, DNA repair, cell proliferation, transcription, translation and miscellaneous, with 31, 13, 6, 8, 18, 10 and 20 genes, respectively. It is noteworthy that, in microarray analysis, the number of genes classified in different functions was not only affected by the treatment (i.e. radiation in our case) performed on samples, but also related to the genes spotted on the chips. For example, if a chip is designed for studying the mechanism of metabolism, most of the probes spotted on this chip will be of this specific functional category. And also, the altered genes selected from this experiment may enrich in the functions related to metabolism. To avoid this artificial error in our analysis, it is necessary to take into consideration the relative numbers of genes on the chip, in biological functions. As in figure 6, the number of altered genes and the expected number of reference genes were calculated against different biological functions. The results showed here provide more reliable information in selecting the regulated functions without the bias from the gene sets that we used on the chips. In consistent with our FACS data, which showed delayed S-phase and extensively G2/M arrest, we found that the regulated genes are enriched in the functions related to cell cycle progression, including the initiation of DNA replication, G2/M transition of mitotic cell cycle, and nuclear division during mitosis (Fig. 7).

To examine the global expression profile of altered genes, we performed

hierarchical clustering analysis based on the similarity of expression patterns of genes across the time course (Fig. 8). Here, red boxes represent genes with increased expression and green boxes represent genes with decreased expression. The magnitude of the change is depicted by the intensity of color. Three major gene expression patterns could be classified in this study, shown by color bar A-C, and the median expression profile of each cluster was plotted with ratio versus time points.

Cluster A (97 genes) contains intermediate to late repressive genes whose response continued throughout the entire time course. This cluster includes the genes in forming mini-chromosome maintenance (MCM) complex which is related to the initiation of DNA synthesis[52], the genes in regulating transcription activity, and the genes in associated with the process of translation. Cluster B (56 genes) showed the early to intermediate inductive pattern whose response also continued throughout the entire time course. Many of the genes which be a member of tumor necrosis family or related to activation of apoptosis were located in this cluster, like TNFSF7 and DR3[53,54], implying the activation of cell death. The genes in cluster C (38 genes) were extensively inhibited at 6 to 12h post-irradiation. Remarkably, half of the genes (18 genes) in cluster C were related to cell cycle progression including CCNB1, CCNB2 and CDC20 whose inhibition corresponding to the G2/M arrest[55,56], or INCENP, STK6 and CENPA whose inhibition may lead to activation of spindle checkpoint and arrest cells at mitotic phase.

Microarray data validation using quantitative RT-PCR

In order to validate the data obtained from microarray, quantitative

real-time RT-PCR (Q-PCR) was performed using SYBR Green I assays. Total RNA from 12 samples (2 independent experiments) were analyzed for the expression of CDKN1A, GADD45A, CDC20, CCNB1, and PCNA, relative to the level of GAPD mRNA in each sample (Table 2). Among these genes, CDKN1A, CDC20 and CCNB1 are genes involved in cell cycle progression and induction of cell-cycle checkpoints; PCNA is known to participate in DNA synthesis phase and maybe related to DNA repair; and GADD45A is now considered to exhibit pleiotropic effects, including cell cycle arrest at G2/M, DNA damage repair, and control of genomic stability[26,55,56,57]. Therefore, we chose these five genes as the target genes for Q-PCR validation (Fig. 9).

Our results showed that there was a strong correlation between log2 transformed ratios determined by Q-PCR and oligonucleotide microarrays. Although microarray appeared to underestimate the expression differences relative to Q-PCR (slope = 0.57, Fig. 10), this effect was consistent and likely to be a result of the kinetic differences between PCR and hybridization reactions[58]. The principle of Q-PCR is to amplify the cDNA of target gene at an optimized condition and to measure the signals at the end of each cycle. By using the housekeeping gene(s) as internal control, the relative abundance of the target gene between two samples could be determined at the linear range of its amplification. On the other hand, microarray measures the expression ratio of genes by competitive hybridization of two samples, and the ratio may not be linear, with the linearity depending on the mRNA abundance of the samples. In addition, when performing the microarray experiments, the measured signal of each spot composes of not only the signal from target gene but also the foreground noises. The noises may due

to the contribution of cross-hybridization, non-specific hybridization, the background signals from supporting materials, etc, and all these factors reduces the reliability and accuracy of microarray data. Hence, Q-PCR provides more faithful results of the ratio of genes between two samples.

IV. DISCUSSION

After 10Gy irradiation, most of the cells were arrested at G2/M phase and sustained for up to 48 hours. In order to study the mechanism(s) of this prolonged G2/M arrest induced by irradiation, the data from temporal gene expression analysis should provide us important hints at the transcriptional level.

Evidence of G2 phase arrest

During G2, the cyclin B/CDC2 complex is held in an inactive state by phosphorylation of CDC2 at two negative regulatory sites, Thr14 and Tyr15. Inactivation of CDC2 via phosphorylation plays a very important role in the control of initiation of mitosis in both fission yeast and animal cells. Dephosphorylation of Thr14 and Tyr15 by CDC25C, which acts as a positive regulator of CDC2, activates the cyclin B/CDC2 complex in late G2 and triggers the initiation of mitosis. Besides, cyclin B/CDC2 complex in turn is thought to phosphorylate and further activate CDC25C, inducing the full activation of cyclin B/CDC2[59].

In mammalian cells, two cyclin B proteins cyclin B1 and B2 are found. We showed that upon the treatment of the U138 cells with IR, the mRNA levels of B-type cyclins were reduced at 6 to 12 hours post irradiation (Table 1). The inhibition of B-type cyclins transcription was proved to have an important role in controlling the entry into mitosis and activating the G2/M checkpoint. For instance, the concentrations of cyclin B2 mRNA were reduced in the treatment of HepG2 cells with 5-fluorouracil or methotrexate through p53-dependent transcription repression and brought to the G2

arrest[60]. The ability of p53 to control mitotic initiation by regulating intracellular cyclin B1 levels also suggested that the B-type cyclins were involved in the G2 checkpoint[55]. However, since U138 cells bearing mutated p53 protein which was proved to be loss of function, the repression of B-type cyclins may be carried out through a p53-independent mechanism or controlled by regulation of its mRNA stability[59]. In either case, cells would have been arrested in G2.

Inhibition of forming mitotic apparatus and M phase checkpoint

If the DNA damage checkpoint is activated, the cells that accumulate in corresponding phase of the cell cycle will increase. In this study, we used propidium iodide staining to measure the DNA contents of cells and also the assessment of cell cycle arrest. The natural limitation of this technique makes it unable to distinguish the mitotic cells from G2 cells. Therefore, we were not able to define whether cells arrested at G2 or M. However, based on our microarray data, the genes involved in G2 arrest and mitotic checkpoint were distinctly identified, and their down-regulation implicated that both events were taking place.

During mitosis, sister chromatids attach via a specialized DNA-protein complex, known as kinetochore, to microtubules emanating from opposite poles of the mitotic spindle. When and only when all kinetochores have bound to microtubules, and under a proper mechanical tension, the mitotic spindle proceeds to pull the sister chromatids apart. A surveillance mechanism, known as spindle checkpoint, is essential for ensuring fidelity in chromosome segregation and for prohibiting premature mitosis[61,62]. In general, in response to unattached kinetochores, the spindle checkpoint halts

the cell cycle progression prior to anaphase. The spindle checkpoint components, like MAD2, BUB1 and BUB3, bind to the unattached kinetochore and form a protein complex with other proteins. This complex catalyzes the formation of CDC20-APC- MAD2 complexes which render CDC20-APC inactive, and arrests cells at metaphase[62].

In our study, the genes whose products were proved to be involved in this checkpoint, such as BUB1, TPX2, STK6 (Aurora A) and INCENP, were repressed on their mRNA levels at 6 to 12 hours after radiation treatment (Table 1). It has been reported, for example, BUB1, a protein kinase which forms complex with BUB3 and phosphorylates BUB3, is responsible for activation of the spindle checkpoint[62]. The WD40 repeat protein CDC20, has been shown to be an activator of the APC complex, binds to and activates the APC, then promotes the execution of anaphase[63]. TPX2, a prominent component of the spindle apparatus, is required for targeting Aurora A to the spindle[64]. Since Aurora A localizes to the centrosomes and spindle, it is able to phosphorylate the spindle-associated proteins and control the spindle formation and maintain its stability. Moreover, the initial actvation of Aurora A in late G2 phase is essential for recruitment of the cyclin B1/ CDK1 complex to centrosomes, and the RNAi study reported by Hirota *et. al.* showed that Aurora A is required for mitotic entry[65]. The inner centromere-like protein (INCENP), which can form complex with Aurora B kinase, helps coordinate chromosome segregation, spindle behavior, and cytokinesis during mitosis[66]. The data here suggest that the repression of these genes may contribute to the increased unattached kinetochore, inactivation of APC complex, instability of spindle, and finally activation of the spindle checkpoint.

In addition, HEC, a novel nuclear protein encoded by the human gene HEC (highly expressed in cancer), was also observed in our study (Table 1). It has been reported that inactivation of HEC by microinjection of specific monoclonal antibodies into cells during interphase severely disturbs the subsequent mitosis[67]. The result suggests that the HEC protein may play an important role in chromosome segregation during M phase. Further, it was found that depletion of Hec1 impaired chromosome congression and caused persistent activation of the spindle checkpoint, indicating the involvement of HEC in spindle checkpoint[68]. Also, members of the Ndc80/Nuf2(CDCA1) complex have been shown in several systems to be important in formation of stable kinetochore-microtubule attachments and chromosome alignment in mitosis. The depletion of Nuf2 by RNAi resulted in a strong prometaphase block with an active spindle checkpoint[69]. Taken together the published literatures and our microarray results, we suggested that both of the G2 and spindle checkpoints were activated in U138 cells after irradiation and contributed to extensive accumulation of the cells at G2/M.

Possible mechanisms of cell death in irradiated U138MG cells

Since there is no evidence for DNA laddering of U138MG cells after irradiation, we interpret these results to indicate that the irradiated U138MG cells did not undergo radiation-induced apoptosis or p53-independent apoptosis. In wild-type cells, p53 plays a role in deciding whether cells should undergo apoptosis or other fates after injury or DNA damage. The activation of cell cycle checkpoint, involving ATM and other associated proteins, leads to p53 phosphorylation and activation. The function of activated p53 is thought to mainly through transcriptional control of target

genes that influence multiple response pathways. Activated p53 also leads to diversity of cellular responses to DNA damage, such as cell cycle arrest, DNA repair and apoptosis[70]. However, in p53-mutated cell line, it is unable to activate p53-dependent apoptosis pathway[71]. Indeed, in our study of U138MG cells, many of the genes involved in p53-dependent apoptosis such as caspases and pro-apoptotic genes were not activated (Table 1). These results, together with the lack of DNA laddering following irradiation, lead us to speculate that the failure to activate apoptosis after irradiation may have contributed, at least partly, to the radio-resistance of the p53-mutated cells.

Following irradiation with a lethal dose, cells would undergo either rapid death (interphase) or delayed death (reproductive)[72]. The delayed reproductive death, also known as mitotic death, is a characteristics of many p53-mutated tumors that are resistant to genotoxic insult[72,73]. On p53 mutated cells, absence of G1/S checkpoint would allow cells to progress through S phase with accumulated DNA damage into G2 arrest, a checkpoint that presumably permits cells more time for repair. It has been shown that during G2 arrest, DNA double strand breaks (DSBs) can be repaired by homologous recombination (HR)[74]. However, cells with excessive chromosome lesions either directly bypass the G2/M checkpoint, starting endocycles from G2 arrest, or are subsequently detected by the spindle checkpoint and present with the features of abortive mitosis or mitotic death[72]. This possible mechanism suggests that the features of mitotic death do not simply represent aberrations of dying cells but are indicative of a switch to amitotic modes of cell survival. This may help us in explaining the phenomena of prolonged G2/M arrest and absence of apoptosis in our study

since the survival of 10 Gy gamma-irradiated U138MG cells is only about 1%[40].

Precautions of interpretations that are based on gene expression profiles alone

In recent years, microarray analysis has become a powerful tool on studying the global gene expression profiles for various purposes. However, there are two common pitfalls that the researchers often face when interpreting microarray results. The first, assuming that the regulations on gene expressions can represent the interactions on proteins or connect directly to the cellular responses. The second, assuming the cell responses should be observed on gene expression profiles. These may lead to the incorrect interpretations on microarray data. Since the regulatory networks in cells are complex, microarray analysis only provides a possible explanation on how cells responding to the stimuli. The interactions and regulations on protein level may not reflect on transcriptional profiles. Therefore, the strong biological inferences can be made from microarray transcriptional data only when they are made within the proper biological and experimental context.

V. CONCLUSION

The present study has substantiated the radiation-induced cell cycle perturbations and cell death on p53-mutated U138 cells. The irradiated cells exhibited a lack of G1/S checkpoint, but a prolonged period of G2/M blockade, while they showed no evidence of apoptotic death. The expressions of genes involved in p53-dependent apoptosis were not altered in our microarray analysis, which supports the loss of p53 function in the cell line. Our temporal microarray data show that the genes involved in regulating the G2/M arrest and mitotic checkpoint were activated, indicating that cells could have been arrested in G2 as well as in mitosis. Further, suppression of several genes vital to the mitotic apparatus strongly suggest that abortive mitosis or mitotic death, rather than interphase apoptosis, accounts for a major mechanism of death in the irradiation population. Based on the temporally global expression data, we have proposed a possible mechanism(s) of radiation-induced cell death for the U138MG cells (Fig. 11).

VI. REFERENCES

1. Kleihues P, Burger PC, Scheithauer BW. The new WHO classification of brain tumours. *Brain Pathol*. 1993;3:255-268.
2. Fine HA, Dear KB, Loeffler JS, et al. Meta-analysis of radiation therapy with and without adjuvant chemotherapy for malignant gliomas in adults. *Cancer*. 1993;71:2585-2597.
3. Huncharek M, Muscat J. Treatment of recurrent high grade astrocytoma; results of a systematic review of 1,415 patients. *Anticancer Res*. 1998; 18:1303-1311.
4. Salcman M, Scholtz H, Kaplan RS, et al. Long-term survival in patients with malignant astrocytoma. *Neurosurgery*. 1994;34:213-219.
5. Salcman M. Survival in glioblastoma: histoical perspective. *Neurosurgery*. 1980;7:435-439.
6. Markert J. Giloblastoma multiforme: introduction. *Cancer J*. 2003; 9:148.
7. Malaise EP, Fertil B, Chavaudra N, et al. Distribution of radiation sensitivities for human tumor cells of specific histological types: comparison of in vitro to in vivo data. *Int J Radiat Oncol Biol Phys*. 1986;12:617-624.
8. Sehgal A. Molecular changes during the genesis of human gliomas. *Semin Surg Oncol*. 1998;14:3-12.
9. Levine AJ. p53, the cellular gatekeeper for growth and division. *Cell*. 1997;88:323-331.
10. Sigal A, Rotter V. Oncogenic mutations of the p53 tumor suppressor:

the demons of the guardian of the genome. *Cancer Res*. 2000;60: 6788-6793.

11. Louis DN. The p53 gene and protein in human brain tumors. *J Neuropathol Exp Neurol*. 1994;53:11-21.
12. Sidransky D, Mikkelsen T, Schwechheimer K, et al. Clonal expansion of p53 mutant cells is associated with brain tumour progression. *Nature*. 1992;355:846-847.
13. Hussain SP, Harris CC. Molecular epidermiology of human cancer: contribution of mutation spectra studies of tumor suppressor genes. *Cancer Res*. 1998;58:4023-4037.
14. Beroud C, Soussi T. p53 gene mutation: software and database. *Nucleic Acids Res*. 1998;26:200-204.
15. de Vries A, Flores ER, Miranda B, et al. Targeted point mutations of p53 lead to dominant-negative inhibition of wild-type p53 function. *Proc Natl Acad Sci*. 2002;99:2948-2953.
16. Lee JM, Bernstein A. p53 mutations increase resistance to ionizing radiation. *Proc Natl Acad Sci*. 1993;90:5742-5746.
17. Li R, Sutphin PD, Schwartz D, et al. Mutant p53 protein expression interferes with p53-independent apoptotic pathways. *Oncogene*. 1998;16:3269-3277.
18. Fridman JS, Lowe SW. Control of apoptosis by p53. *Oncogene*. 2003;22:9030-9040.
19. Elledge SJ. Cell cycle checkpoints: preventing an identity crisis. *Science*. 1996;274:1664-1672.

20. Zhou BB, Elledge SJ. The DNA damage response: putting checkpoints in perspective. *Nature*. 2000;408:433-439.

21. Iliakis G, Wang Y, Guan J, et al. DNA damage checkpoint control in cells exposed to ionizing radiation. *Oncogene*. 2003;22:5834-5847.

22. Canman CE, Lim DS, Cimprich KA, et al. Activation of the ATM kinase by ionizing radiation and phosphorylation of p53. *Science*. 1998;281:1677-1679.

23. Harper JW, Adami GR, Wei N, et al. The p21 Cdk-interacting protein Cip1 is a potent inhibitor of G1 cyclin-dependent kinases. *Cell*. 1993;75:805-816.

24. Chan TA, Hermeking H, Lengauer C, et al. 14-3-3Sigma is required to prevent mitotic catastrophe after DNA damage. *Nature*. 1999; 401:616-620.

25. Peng CY, Graves PR, Thoma RS, et al. Mitotic and G2 checkpoint control: regulation of 14-3-3 protein binding by phosphorylation of Cdc25C on serine-216. *Science*. 1997;277:1501-1505.

26. Rich T, Allen RL, Wyllie AH. Defying death after DNA damage. *Nature*. 2000;407:777-783.

27. Kannan K, Amariglio N, Rechavi G, et al. DNA microarrays identification of primary and secondary target genes regulated by p53. *Oncogene*. 2001;20:2225-2234.

28. Sionov RV, Haupt Y. The cellular response to p53: the decision between life and death. *Oncogene*. 1999;18:6145-6157.

29. Kuerbitz SJ, Plunkett BS, Walsh WV, et al. Wild-type p53 is a cell cycle

checkpoint determinant following irradiation. *Proc Natl Acad Sci*. 1992;89:7491-7495.

30. Schulze A, Downward J. Navigating gene expression using microarrays - a technology review. *Nat Cell Biol*. 2001;3:E190-E195.

31. Celis JE, Kruhoffer M, Gromova I, et al. Gene expression profiling: monitoring transcription and translation products using DNA microarrays and proteomics. *FEBS Lett*. 2000;480:2-16.

32. Pease AC, Solas D, Sullivan EJ, et al. Light-generated oligonucleotide arrays for rapid DNA sequence analysis. *Proc Natl Acad Sci*. 1994; 91:5022-5026.

33. Hughes TR, Mao M, Jones AR, et al. Expression profiling using microarrays fabricated by an ink-jet oligonucleotide synthesizer. *Nat Biotechnol*. 2001;19:342-347.

34. Blanchard AP, Kaiser RJ, Hood LE. High-density oligonucleotide arrays. *Biosens Bioelectron*. 1996;11:687-690.

35. Ross DT, Scherf U, Eisen MB, et al. Systematic variation in gene expression patterns in human cancer cell lines. *Nat Genet*. 2000; 24:227-235.

36. Stankovic T, Hubank M, Cronin D, et al. Microarray analysis reveals that TP53- and ATM-mutant B-CLLs share a defect in activating proapoptotic responses after DNA damage but are distinguished by major differences in activating prosurvival responses. *Blood*. 2004;103:291-300.

37. Elledge SJ, Davis RW, Lockhart DJ. Transcriptional regulation and function during the human cell cycle. *Nat Genet*. 2001;27:48-54.

38. Tada M, Matsumoto R, Iggo RD, et al. Selectively sensitivity to radiation of cerebral glioblastomas harboring p53 mutations. *Cancer Res*. 1998;58:1793-1797.

39. Asaoka K, Tada M, Sawamura Y, et al. Dependence of efficient adenoviral gene delivery in malignant glioma cells on the expression levels of the Coxsackievirus and adenovirus receptor. *J Neurosurg*. 2000;92:1002-1008.

40. Hsiao YY. The effects of radiation on p53-mutated glioma cells using cDNA microarray technique. *Master thesis* 2003. Institute of Radiological Sciences, National Yang-Ming University.

41. Gong J, Traganos F, Darzynkiewicz Z. A selective procedure for DNA extraction from apoptotic cells applicable for gel electrophoresis and flow cytometry. *Anal Biochem*. 1994;218:314-319.

42. Draghici S, Khatri P, Bhavsar P, et al. Onto-Tools, the toolkit of the modern biologist: Onto-Express, Onto-Compare, Onto-Design and Onto-Translate. *Nucleic Acids Res*. 2003;31:3775-3781.

43. Zhang B, Schmoyer D, Kirov S, et al. GOTree Machine (GOTM): a web-based platform for interpreting sets of interesting genes using Gene Ontology hierarchies. *BMC Bioinformatics*. 2004;5:16.

44. Livak KJ, Schmittgen TD. Analysis of relative gene expression data using real-time quantitative PCR and the 2(-Delta Delta C(T)) Method. *Methods*. 2001;25:402-408.

45. Bustin SA. Absolute quantification of mRNA using real-time reverse transcription polymerase chain reaction assays. *J Mol Endocrinol*. 2000;25:169-193.

46. Khodarev NN, Sokolova IA, Vaughan AT. Mechanisms of induction of apoptotic DNA fragmentation. *Int J Radiat Biol*. 1998;73:455-467.

47. Kiechle FL, Zhang X. Apoptosis: biochemical aspects and clinical implications. *Clin Chim Acta*. 2002;326:27-45.

48. Yao KC, Komata T, Kondo Y, et al. Molecular response of human glioblastoma multiforme cells to ionizing radiation: cell cycle arrest, modulation of the expression of cyclin-dependent kinase inhibitors, and autophagy. *J Neurosurg*. 2003;98:378-384.

49. Yount GL, Haas-Kogan DA, Vidair CA, et al. Cell cycle synchrony unmasks the influence of p53 function on radiosensitivity of human glioblastoma cells. *Cancer Res*. 1996;56:500-506.

50. Dudoit S, Yang YH, Callow MJ, et al. Statistical methods for identifying differentially expressed genes in replicated cDNA microarray experiments. *Statistica Sinica*. 2002;12:111-139.

51. Khatri P, Draghici S, Ostermeier GC, et al. Profiling gene expression using onto-express. *Genomics*. 2002;79:266-270.

52. Bailis JM, Forsburg SL. MCM proteins: DNA damage, mutagenesis and repair. *Curr Opin Genet Dev*. 2004;14:17-21.

53. Reed JC. Mechanisms of apoptosis. *Am J Pathol*. 2000;157:1415-1430.

54. Marsters SA, Sheridan JP, Donahue CJ, et al. Apo-3, a new member of the tumor necrosis factor receptor family, contains a death domain and activates apoptosis and NF-kappa B. *Curr Biol*. 1996;6:1669-1676.

55. Innocente SA, Abrahamson JL, Cogswell JP, et al. p53 regulates a G2 checkpoint through cyclin B1. *Proc Natl Acad Sci*. 1999;96:2147-2152.

56. Chung E, Chen RH. Phosphorylation of Cdc20 is required for its inhibition by the spindle checkpoint. *Nat Cell Biol*. 2003;5:748-753.

57. Chen IT, Smith ML, O'Connor PM, et al. Direct interaction of Gadd45 with PCNA and evidence for competitive interaction of Gadd45 and p21Waf1/Cip1 with PCNA. *Oncogene*. 1995;11:1931-1937.

58. Yuen T, Wurmbach E, Pfeffer RL, et al. Accuracy and calibration of commercial oligonucleotide and custom cDNA microarrays. *Nucleic Acids Res*. 2002;30:e48.

59. Smits VA, Medema RH. Checking out the G(2)/M transition. *Biochim Biophys Acta*. 2001;1519:1-12.

60. Krause K, Wasner M, Reinhard W, et al. The tumour suppressor protein p53 can repress transcription of cyclin B. *Nucleic Acids Res*. 2000;28:4410-4418.

61. Straight AF. Cell cycle: checkpoint proteins and kinetochores. *Curr Biol*. 1997;7:R613-R616.

62. Amon A. The spindle checkpoint. *Curr Opin Genet Dev*. 1999;9:69-75.

63. Burke DJ. Complexity in the spindle checkpoint. *Curr Opin Genet Dev*. 2000;10:26-31.

64. Kufer TA, Sillje HH, Korner R, et al. Human TPX2 is required for targeting Aurora-A kinase to the spindle. *J Cell Biol*. 2002;158:617-623.

65. Hirota T, Kunitoku N, Sasayama T, et al. Aurora-A and an interacting activator, the LIM protein Ajuba, are required for mitotic commitment in human cells. *Cell*. 2003;114:585-598.

66. Pereira G, Schiebel E. Separase regulates INCENP-Aurora B anaphase

spindle function through Cdc14. *Science*. 2003;302:2120-2124.

67. Chen Y, Riley DJ, Chen PL, et al. HEC, a novel nuclear protein rich in leucine heptad repeats specifically involved in mitosis. *Mol Cell Biol*. 1997;17:6049-6056.

68. Martin-Lluesma S, Stucke VM, Nigg EA. Role of Hec1 in spindle checkpoint signaling and kinetochore recruitment of Mad1/Mad2. *Science*. 2002;297:2267-2270.

69. DeLuca JG, Howell BJ, Canman JC, et al. Nuf2 and Hec1 are required for retention of the checkpoint proteins Mad1 and Mad2 to kinetochores. *Curr Biol*. 2003;13:2103-2109.

70. Fei P, El-Deiry WS. P53 and radiation responses. *Oncogene*. 2003;22: 5774-5783.

71. Yasumoto J, Imai Y, Takahashi A, et al. Analysis of apoptosis-related gene expression after X-ray irradiation in human tongue squamous cell carcinoma cells harboring wild-type or mutated p53 gene. *J Radiat Res*. 2003;44:41-45.

72. Erenpreisa J, Cragg MS. Mitotic death: a mechanism of survival? A review. *Cancer Cell Int*. 2001;1:1-7.

73. Castedo M, Perfettini JL, Roumier T, et al. Cell death by mitotic catastrophe: a molecular definition. *Oncogene*. 2004;23:2825-2837.

74. Valerie K, Povirk LF. Regulation and mechanisms of mammalian double-strand break repair. *Oncogene*. 2003;22:5792-5812.

VII. TABLES

Table 1. Differential Gene Expression Identified by Microarray Analysis

	MA1					MA2					
Time(hr)	0.5	6	12	24	36	0.5	6	12	24	36	Accession
I. Cell Cycle (31)											
Cluster A											
CCT2	0.94	0.87	0.94	0.73	0.72	0.92	0.92	0.91	0.84	0.64	AF026166
MCM2	0.98	1.10	1.00	0.67	0.56	0.98	0.98	1.07	0.75	0.48	NM_004526
MCM3	1.03	1.03	1.03	0.52	0.45	1.04	1.05	1.04	0.56	0.38	D38073
MCM5	0.96	1.05	1.08	0.72	0.61	1.03	1.15	1.00	0.69	0.51	BC000142
MCM6	0.94	0.88	0.96	0.53	0.34	1.03	0.97	0.99	0.49	0.32	D84557
MCM7	1.03	1.13	1.05	0.71	0.59	1.00	1.04	1.05	0.78	0.51	NM_005916
POLE3	0.97	0.93	1.00	0.74	0.71	0.94	0.88	1.00	0.94	0.70	AK074762
HSPCA	1.03	0.87	0.86	0.59	0.62	0.90	0.69	0.81	0.82	0.49	AF028832
Cluster B											
TGFA	1.06	0.99	1.52	1.96	2.13	0.95	1.07	2.07	2.19	2.47	NM_003236
CDKN1A	1.10	1.03	1.44	1.37	1.27	1.18	1.02	1.35	1.48	2.02	U03106
SESN2	0.80	1.18	1.79	2.08	1.59	1.15	1.08	1.59	1.82	2.72	AY123223
ASNS	1.00	1.10	1.99	3.52	2.68	0.98	0.96	1.88	2.67	3.43	BC014621
CCNG2	0.97	1.00	1.08	1.37	1.33	1.01	0.90	1.07	1.36	1.81	NM_004354
Cluster C											
CDKN3	1.01	0.66	0.60	0.85	1.28	0.90	0.58	0.47	0.79	1.26	AK098653
BUB1	0.97	0.65	0.70	0.99	1.03	0.92	0.49	0.59	0.79	0.96	AF046078
KPNA2	0.97	0.59	0.59	0.95	1.27	0.93	0.47	0.54	1.04	1.15	U09559
CCNB1	0.97	0.43	0.52	0.84	1.17	0.86	0.44	0.44	0.81	1.17	BC006510
CCNB2	0.94	0.55	0.55	0.86	1.18	1.03	0.52	0.54	0.94	1.36	AL080146
CDC20	0.95	0.47	0.48	0.82	1.25	1.06	0.49	0.45	0.85	1.24	BC000624
CDCA1	0.95	0.68	0.91	1.35	1.41	0.95	0.59	0.74	1.09	1.31	AK093348
CDCA8	0.95	0.56	0.66	0.88	1.06	0.99	0.58	0.75	0.90	1.07	BC001651
MKI67	1.14	0.67	0.88	1.24	1.33	1.10	0.52	0.53	0.82	1.05	X65550
HEC	0.95	0.49	0.72	0.98	1.08	0.95	0.44	0.58	0.89	1.09	BC035617
INCENP	0.95	0.70	0.76	1.00	0.93	1.01	0.58	0.76	0.94	0.98	AK056195
STK6	0.98	0.46	0.52	0.87	1.15	0.94	0.37	0.55	0.92	1.08	BC006423
TPX2	0.95	0.67	0.79	0.98	1.09	0.89	0.67	0.70	1.00	1.12	BC004136
PTTG1	0.94	0.76	0.56	0.82	1.02	1.03	0.70	0.57	0.81	1.10	AJ223953
PTTG2	0.98	0.72	0.65	0.85	1.07	0.99	0.74	0.57	0.83	1.08	NM_006607
PTTG3	0.99	0.74	0.56	0.82	1.03	1.10	0.74	0.54	0.81	1.06	NM_021000
ASK	0.91	0.64	0.72	0.85	1.00	0.89	0.54	0.56	0.82	1.07	AF160876
TOPK	0.94	0.72	0.91	0.91	0.91	0.90	0.58	0.73	0.99	0.89	AB027249

(*Continued on next page*)

Table 1. *(Continued)*

	MA1					MA2					
Time(hr)	0.5	6	12	24	36	0.5	6	12	24	36	Accession
II. Apoptosis (13)											
Cluster A											
CTNNAL1	0.95	0.86	0.95	0.72	0.72	0.94	0.87	0.88	0.82	0.70	NM_003798
CASP4	0.99	0.94	1.00	0.75	0.70	1.00	0.96	0.99	0.84	0.66	U28978
CYCS	1.01	0.94	0.99	0.76	0.64	0.95	0.94	0.93	0.81	0.60	BC009607
NCL	1.00	0.97	0.85	0.69	0.62	0.96	1.02	0.82	0.73	0.60	NM_005381
Cluster B											
TNFSF7	1.01	1.22	1.48	1.91	1.78	1.02	1.22	1.51	2.13	2.57	S69339
TNFRSF25	1.04	1.21	1.11	1.66	1.57	1.13	1.35	1.20	1.41	1.70	NM_148965
C20orf97	0.93	0.99	2.33	4.26	2.61	1.09	1.04	2.45	3.84	5.39	AK026945
UNC5B	1.24	1.19	1.80	4.24	3.91	0.93	1.10	1.79	3.02	5.22	NM_170744
FDXR	1.02	1.37	1.33	1.28	1.15	1.02	1.43	1.13	1.15	1.43	NM_004110
GSN	1.04	1.09	1.21	1.46	1.49	0.96	1.18	1.16	1.31	1.63	NM_000177
TIMP3	1.05	1.44	1.39	2.01	2.91	0.98	1.70	1.26	1.77	2.99	S78453
LGALS3	1.07	1.13	1.22	1.75	1.67	0.95	1.16	1.33	1.47	2.35	AB006780
Cluster C											
BIRC5	0.99	0.80	0.60	0.80	1.02	1.02	0.73	0.62	0.87	1.07	U75285
III. DNA Repair (6)											
Cluster A											
UNG	1.02	1.02	1.06	0.62	0.53	0.99	1.02	1.05	0.59	0.54	NM_080911
PCNA	1.03	1.11	1.21	0.64	0.53	0.96	1.18	1.02	0.70	0.52	BC000491
MSH6	1.05	1.07	1.11	0.71	0.63	0.95	1.09	0.99	0.74	0.66	U28946
Cluster B											
DDB2	0.97	1.41	1.58	1.44	1.14	0.86	1.30	1.48	1.52	1.64	U18300
RRM2B	1.09	1.35	1.80	1.73	1.64	0.99	1.82	1.44	1.88	2.17	BC042468
Cluster C											
HMGB2	0.97	0.70	0.94	1.17	0.96	1.05	0.65	0.76	1.11	1.27	X62534

(*Continued on next page*)

Table 1. (*Continued*)

	MA1					MA2					
Time(hr)	0.5	6	12	24	36	0.5	6	12	24	36	Accession
IV. Growth & Proliferation (8)											
Cluster A											
EDN1	0.94	0.78	0.91	0.76	0.69	0.93	0.98	0.82	0.64	0.52	Y00749
DENR	0.93	0.90	0.97	0.68	0.65	0.84	0.69	0.84	0.72	0.50	AB014731
IFRD2	0.96	0.87	0.84	0.70	0.65	1.05	0.90	0.95	0.82	0.63	NM_006764
CYR61	0.95	0.57	0.70	0.57	0.39	0.95	0.67	0.69	0.49	0.47	BC016952
CTPS	1.00	0.89	0.91	0.71	0.64	0.98	1.02	1.04	0.90	0.56	NM_001905
USP1	1.00	0.94	1.07	0.77	0.62	0.98	0.86	1.09	0.94	0.72	AF117386
Cluster B											
BCL6	1.08	1.18	1.31	1.22	1.45	1.26	1.03	1.45	1.31	1.66	Z21943
IGF2R	1.06	1.23	1.32	1.47	1.52	1.14	1.39	1.03	1.07	1.55	Y00285
V. Transcription (18)											
Cluster A											
HIST1H1E	0.90	0.65	0.95	0.68	0.35	0.92	0.54	0.66	0.53	0.37	NM_005321
HIST1H2AH	1.02	0.76	0.86	0.82	0.56	0.95	0.73	0.70	0.60	0.46	NM_080596
HIST1H4C	0.85	0.74	1.10	0.68	0.29	0.80	0.61	0.75	0.56	0.35	AY128656
HIST1H4L	0.97	0.81	1.03	0.72	0.36	0.84	0.67	0.78	0.59	0.38	NM_003546
HIST1H4I	0.89	0.75	1.19	0.75	0.38	0.83	0.72	0.79	0.59	0.45	NM_003495
HIST2H2AC	0.95	0.77	0.92	0.82	0.43	1.01	0.59	0.64	0.45	0.38	NM_003517
HIST3H2A	0.97	0.79	0.92	0.84	0.57	0.92	0.75	0.75	0.61	0.55	AY131974
SFRS3	0.97	0.83	0.89	0.73	0.60	0.91	0.76	0.80	0.78	0.56	BC000914
SFRS3	1.04	0.89	0.90	0.75	0.68	0.94	0.75	0.82	0.85	0.62	NM_003017
KLF2	0.98	0.68	0.96	0.83	0.69	0.99	0.72	0.87	0.71	0.65	AF134053
LOC55924	0.97	0.81	0.68	0.59	0.60	0.98	0.84	0.69	0.62	0.65	AK055667
UHRF1	0.97	0.95	0.97	0.73	0.64	0.97	1.00	0.94	0.74	0.52	AF129507
SFRS10	0.96	0.80	0.85	0.73	0.71	0.99	0.77	0.87	0.81	0.70	BC000160
Cluster B											
MAFB	0.95	1.12	0.95	1.13	1.68	1.02	1.05	1.00	1.08	1.74	NM_005461
HDAC10	1.00	1.24	1.13	1.40	1.45	1.09	1.36	0.96	1.15	1.42	NM_032019
ATBF1	1.14	1.37	1.40	1.55	1.49	1.19	1.27	1.09	1.40	1.55	NM_006885
Cluster C											
HIST1H2BD	0.92	0.60	0.70	0.63	0.80	0.89	0.70	0.81	0.70	0.86	NM_021063
EGR1	1.12	0.33	0.25	0.45	0.29	1.43	0.39	0.48	0.39	0.72	M62829

(*Continued on next page*)

Table 1. (*Continued*)

	MA1					MA2					
Time(hr)	0.5	6	12	24	36	0.5	6	12	24	36	Accession
VI. Translation (10)											
Cluster A											
PSMD7	1.01	0.94	0.88	0.68	0.66	0.92	0.83	1.00	0.93	0.69	BC012606
EIF4E	0.92	0.78	0.82	0.67	0.66	0.86	0.66	0.77	0.78	0.60	M15353
EIF5	1.03	0.77	0.71	0.55	0.62	0.93	0.72	0.75	0.73	0.65	BC032866
ICMT	0.97	0.96	1.01	0.75	0.63	0.97	0.97	0.90	0.80	0.59	BC028168
TCP1	0.95	0.95	0.90	0.73	0.72	0.97	0.84	0.97	0.88	0.67	BC000665
CCT6A	0.96	0.94	0.92	0.71	0.73	0.91	0.92	0.80	0.75	0.57	L27706
HSPD1	0.92	0.91	0.86	0.61	0.61	0.97	0.78	0.92	0.85	0.56	BC002676
PPIL1	0.89	0.83	0.94	0.81	0.73	1.01	0.86	1.04	0.88	0.73	BC003048
EEF1E1	1.04	0.91	1.07	0.76	0.64	0.91	0.84	0.96	0.80	0.56	BC005291
BZW1	0.93	0.82	0.82	0.74	0.74	0.89	0.81	0.86	0.89	0.73	D13630
VII. Miscellaneous (20)											
Cluster A											
MMP1	1.03	0.81	0.71	0.43	0.43	0.97	0.73	0.69	0.60	0.55	X54925
MMP3	0.95	1.02	0.97	0.68	0.60	0.93	0.89	0.81	0.78	0.62	X05232
HAT1	1.02	1.05	1.19	0.72	0.68	0.93	0.90	1.12	0.91	0.60	NM_003642
PSMB6	1.07	1.09	0.94	0.76	0.71	0.92	0.88	0.95	0.83	0.62	BC000835
MT1A	0.92	0.83	0.75	0.60	0.53	0.91	0.81	0.77	0.71	0.67	BC029475
MT1B	0.91	0.79	0.58	0.51	0.45	0.98	0.75	0.61	0.56	0.54	AY168638
MT1G	0.95	0.78	0.60	0.50	0.44	0.98	0.76	0.60	0.56	0.55	BC020757
MT1H	0.93	0.77	0.63	0.58	0.48	0.99	0.83	0.68	0.65	0.59	BC008408
MT1J	0.95	0.80	0.60	0.52	0.45	0.96	0.77	0.61	0.56	0.56	NM_175622
MT1X	0.94	0.83	0.62	0.50	0.44	0.98	0.78	0.61	0.55	0.54	NM_005952
MT2A	0.96	0.80	0.64	0.54	0.45	0.94	0.80	0.64	0.59	0.57	NM_005953
GLIPR1	0.99	0.87	0.70	0.49	0.42	0.95	0.72	0.78	0.60	0.41	U16307
GLIPR1	0.92	0.73	0.89	0.59	0.56	0.97	0.90	0.76	0.64	0.47	NM_006851
CKAP2	0.86	0.65	0.65	0.82	0.98	0.85	0.50	0.59	0.83	1.10	Y15758
Cluster B											
GSN	1.04	1.09	1.21	1.46	1.49	0.96	1.18	1.16	1.31	1.63	NM_000177
TNC	1.14	1.12	1.21	1.42	1.42	0.98	1.19	0.93	1.10	1.47	M55618
EFNB1	1.08	0.85	0.99	1.29	1.57	1.04	1.05	1.16	1.28	1.46	BC016649
THBS1	0.80	1.33	1.50	1.33	1.74	0.97	1.76	1.39	1.76	1.65	X04665
Cluster C											
CENPA	1.00	0.55	0.64	1.06	1.23	1.01	0.52	0.64	0.93	1.22	U14518
UBE2C	1.00	0.72	0.81	1.25	1.47	0.96	0.67	0.78	1.15	1.48	BC016292

Table 2. Primers Used in Quantitative RT-PCR

Gene Name	cyclin-dependent kinase inhibitor 1A (p21, Cip1)	Amplicon	97
Symbol	CDKN1A	Genebank accession	NM_000389.2
Forward (5' → 3')	CCTCATCCCGTGTTCTCCTTT	GC (%) = 52	Tm (°C) = 54.4
Reverse (3' → 5')	GTACCACCCAGCGGACAAGT	GC (%) = 60	Tm (°C) = 55.9
Gene Name	growth arrest and DNA-damage-inducible, alpha	Amplicon	83
Symbol	GADD45A	Genebank accession	NM_001924.2
Forward (5' → 3')	TCAGCGCACGATCACTGTC	GC (%) = 58	Tm (°C) = 53.2
Reverse (3' → 5')	CCAGCAGGCACAACACCAC	GC (%) = 63	Tm (°C) = 55.4
Gene Name	cyclin B1	Amplicon	157
Symbol	CCNB1	Genebank accession	NM_031966.2
Forward (5' → 3')	TCTGGATAATGGTGAATGGACA	GC (%) = 41	Tm (°C) = 51.1
Reverse (3' → 5')	CGATGTGGCATACTTGTTCTTG	GC (%) = 45	Tm (°C) = 53.0
Gene Name	CDC20 cell division cycle 20 homolog (S. cerevisiae)	Amplicon	91
Symbol	CDC20	Genebank accession	NM_001255.1
Forward (5' → 3')	GCCCACCAAGAAGGAACATC	GC (%) = 55	Tm (°C) = 53.8
Reverse (3' → 5')	TTTTCCACTGAGCCGAAGGA	GC (%) = 50	Tm (°C) = 51.8
Gene Name	proliferating cell nuclear antigen	Amplicon	76
Symbol	PCNA	Genebank accession	NM_002592.2
Forward (5' → 3')	AGGCACTCAAGGACCTCATCA	GC (%) = 52	Tm (°C) = 54.4
Reverse (3' → 5')	GAGTCCATGCTCTGCAGGTTT	GC (%) = 52	Tm (°C) = 54.4
Gene Name	beta-2-microglobulin	Amplicon	101
Symbol	B2M	Genebank accession	NM_004048.1
Forward (5' → 3')	ATGAGTATGCCTGCCGTGTGA	GC (%) = 52	Tm (°C) = 54.4
Reverse (3' → 5')	GGCATCTTCAAACCTCCATG	GC (%) = 50	Tm (°C) = 51.8
Gene Name	glyceraldehyde-3-phosphate dehydrogenase	Amplicon	86
Symbol	GAPD	Genebank accession	NM_002046.2
Forward (5' → 3')	TGCACCACCAACTGCTTAGC	GC (%) = 55	Tm (°C) = 53.8
Reverse (3' → 5')	GGCATGGACTGTGGTCATGAG	GC (%) = 57	Tm (°C) = 56.3
Gene Name	hypoxanthine phosphoribosyltransferase 1	Amplicon	94
Symbol	HPRT1	Genebank accession	NM_000194.1
Forward (5' → 3')	TGACACTGGCAAAACAATGCA	GC (%) = 43	Tm (°C) = 50.5
Reverse (3' → 5')	GGTCCTTTTCACCAGCAAGCT	GC (%) = 52	Tm (°C) = 54.4

VIII. FIGURES

(A)

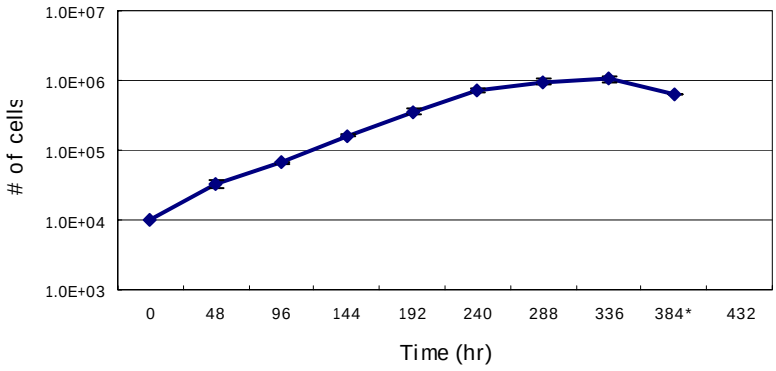

(B)

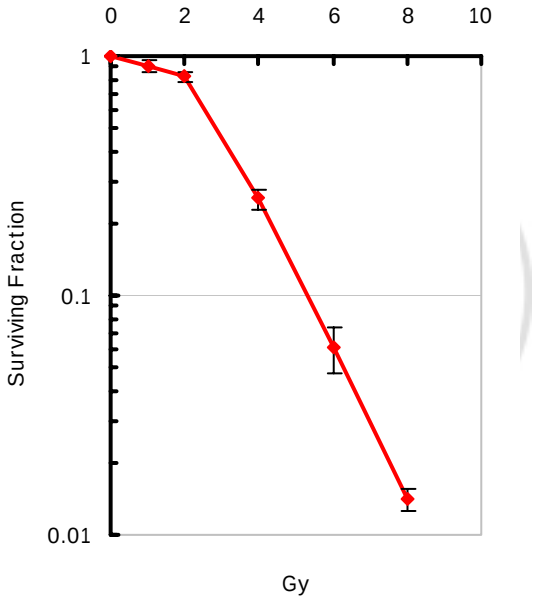

Figure 1. Growth kinetics and survival curve of U138 cell line. (A) Each time point represented by the average of triplicate dishes. After calculating the increasing population against incubation time, the population-doubling time of U138 cells is about 39.33 hours. (B) The cell killing which caused by different dose (ranging from 1 to 8 Gy) was investigated, and the survival fraction of U138 cell receiving 8 Gy irradiation was about 1.41%.

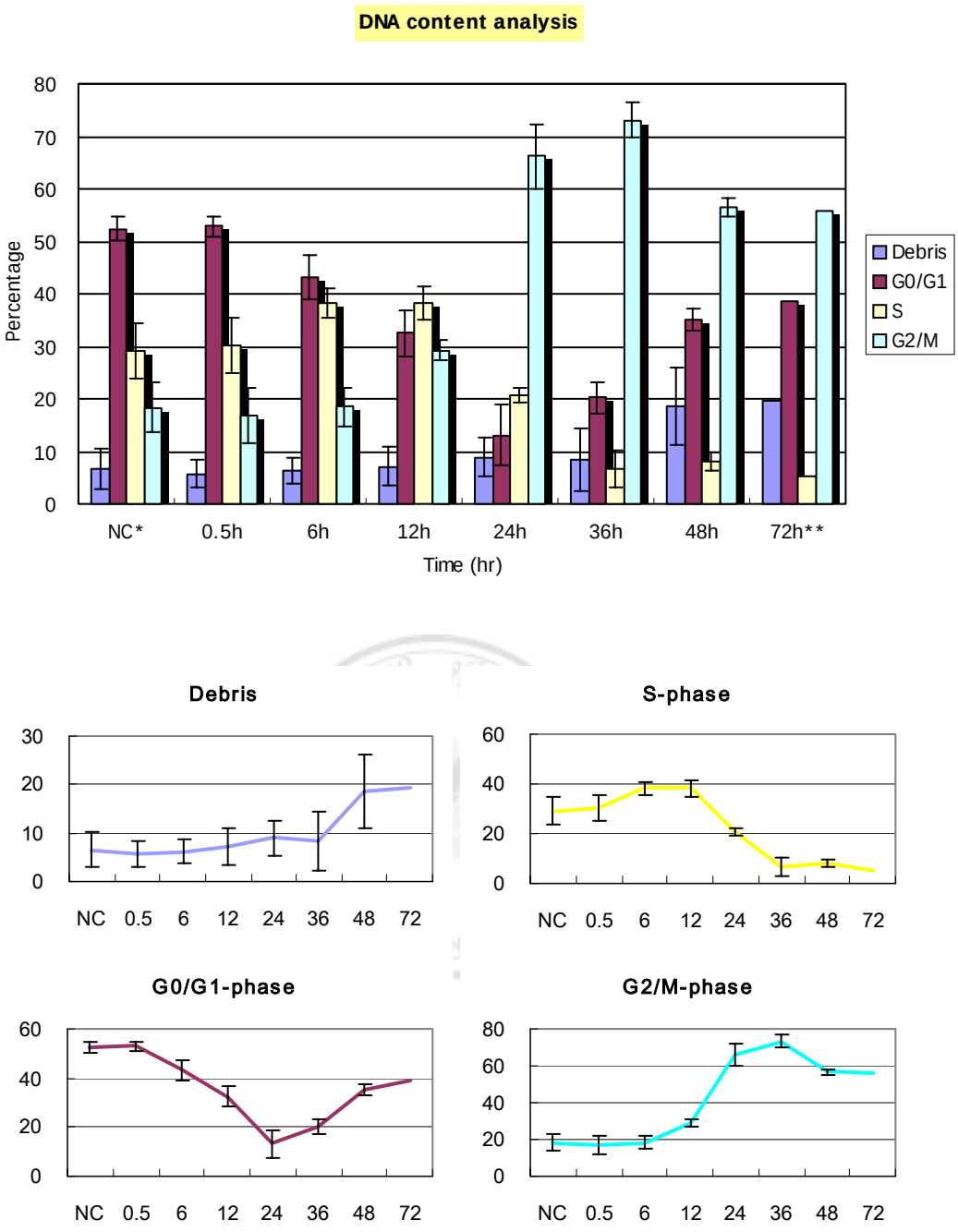

Figure 2. Cell cycle changes in U138 cells after irradiation. The proportion of cells in each part of the cell cycle for this cell line is shown. Cells after irradiation with 10Gy of Co-60 were harvested at different time points and were analyzed with FACS by the use of PI dye. The data showed here are repeated at least three times, except the 72h. NC refers to the negative control, which are non-irradiated cells.

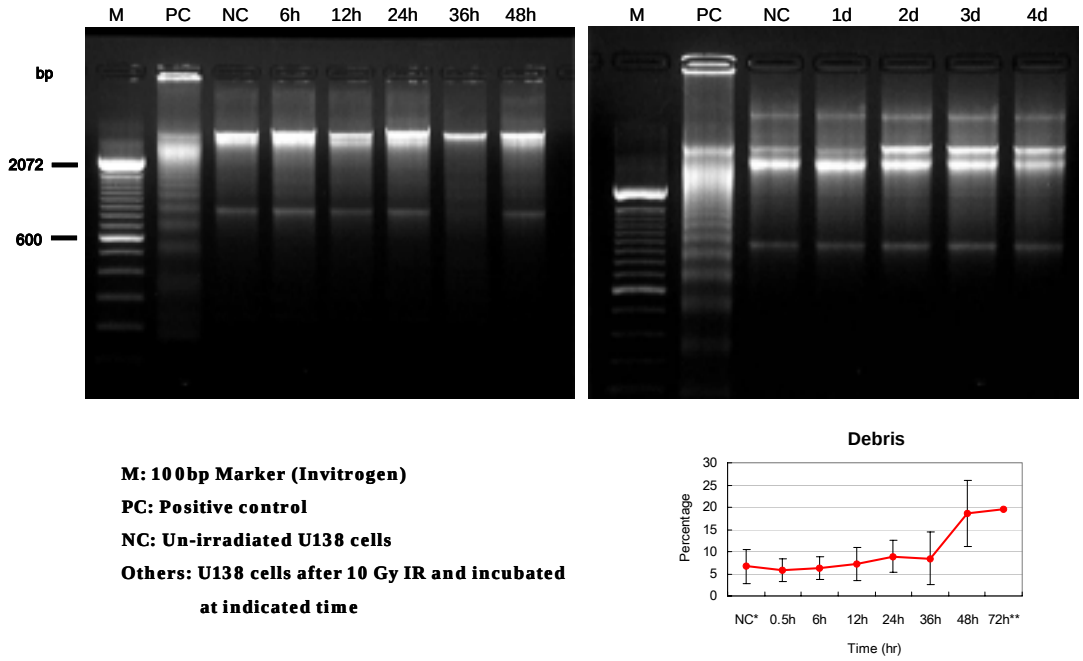

Figure 3. DNA laddering assay in detecting radiation induced apoptosis. In this study, cells after 10 Gy irradiation were harvested at indicated time points and examined for DNA fragmentation through agarose gel electrophoresis. 3 μg of DNA were extracted for each experiment to be loaded on the gel. Molecular weight standards indicating number of base pairs are given.

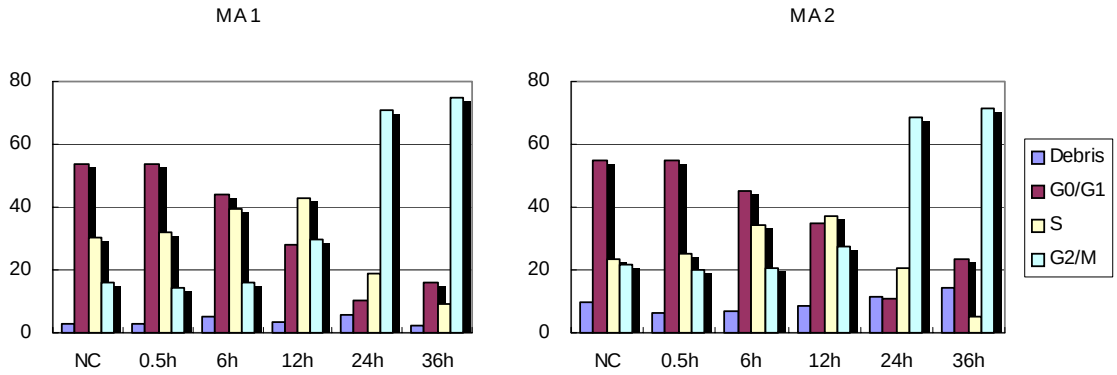

Figure 4. FACS analysis on microarray samples. The DNA content in two independent experiments was investigated using flow cytometry, and the results showed here was in consistent with previous data.

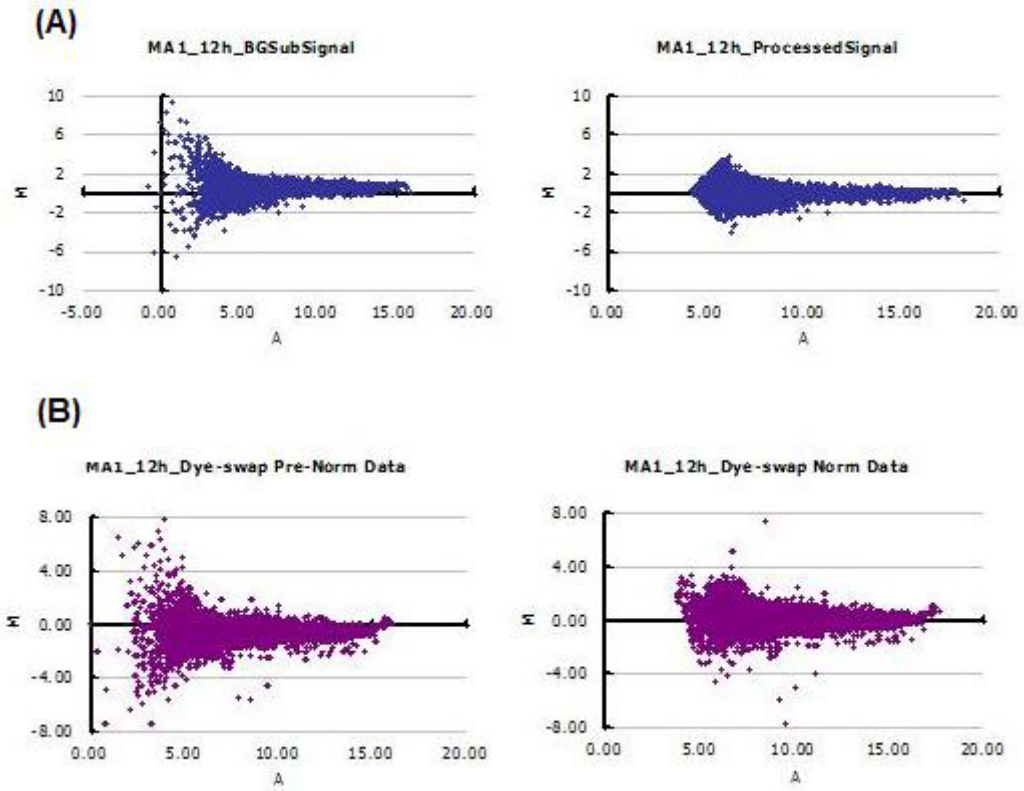

Figure 5. The distribution of microarray data represented with M-A plots. Using just the ratios or log ratios to visualize the data does not enable us to see the systematic dependence of the ratio on intensity values. The M-A plots, which can show the intensity-dependant ratio of raw microarray data, were used to represent the distribution of the ratio of the genes (M) and the relative amount of genes (A). It's clear that M noise is greater as A decreases, and the data processed with normalization eliminate the noise produced by the faint spots.

As defined in the reported data:

$A = 1/2*(\log_2(Cy5) + \log_2(Cy3))$

$M = \log_2(Cy5 / Cy3)$

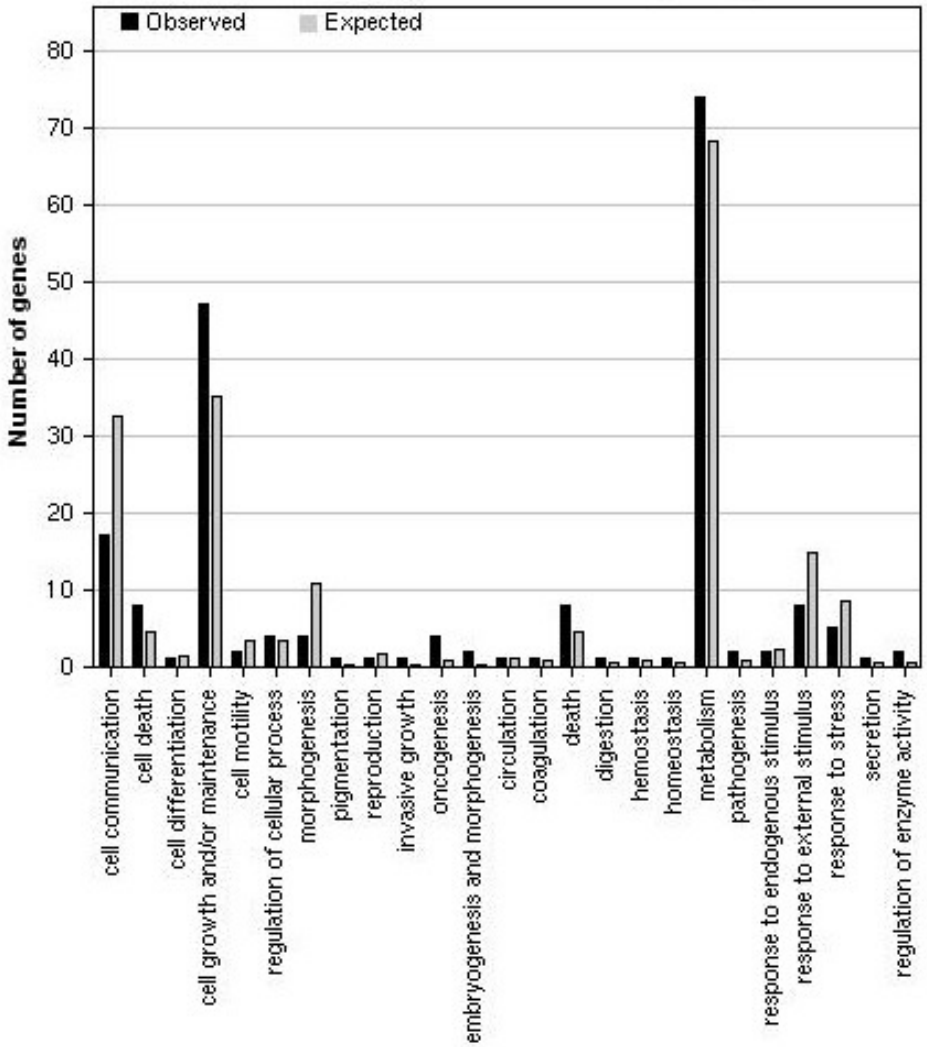

Figure 6. Functional grouping performed with differentially expressed genes. The black bar indicated the number of genes observed in the DEGenes list, and the gray bar indicated the number of genes in the reference list, which contains all probes on the chip.

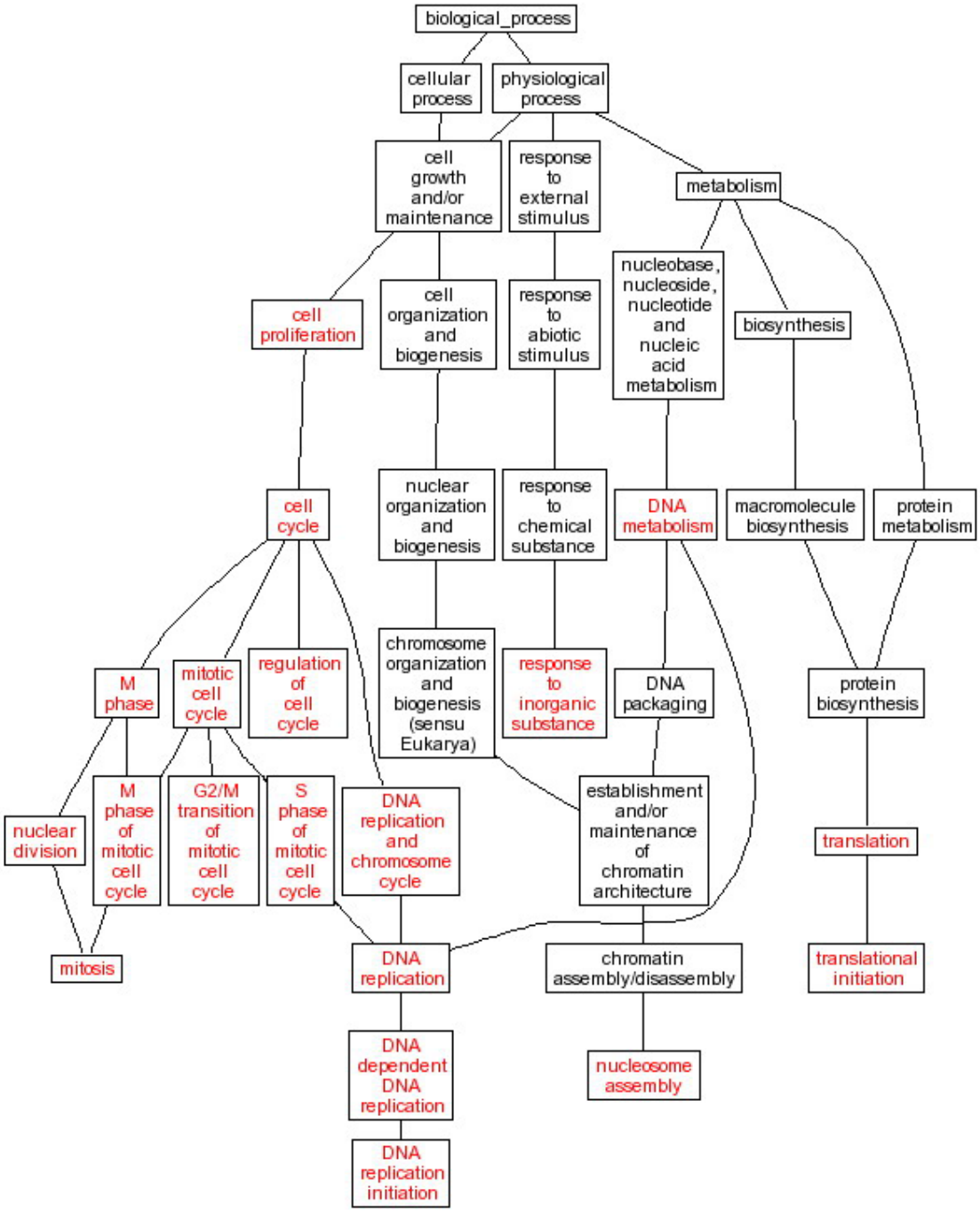

Figure 7. DAG view of enriched GO categories. The enriched GO categories are brought together and visualized as a Directed Acyclic Graph (DAG). Categories in red are enriched ones while those in black are non-enriched patterns.

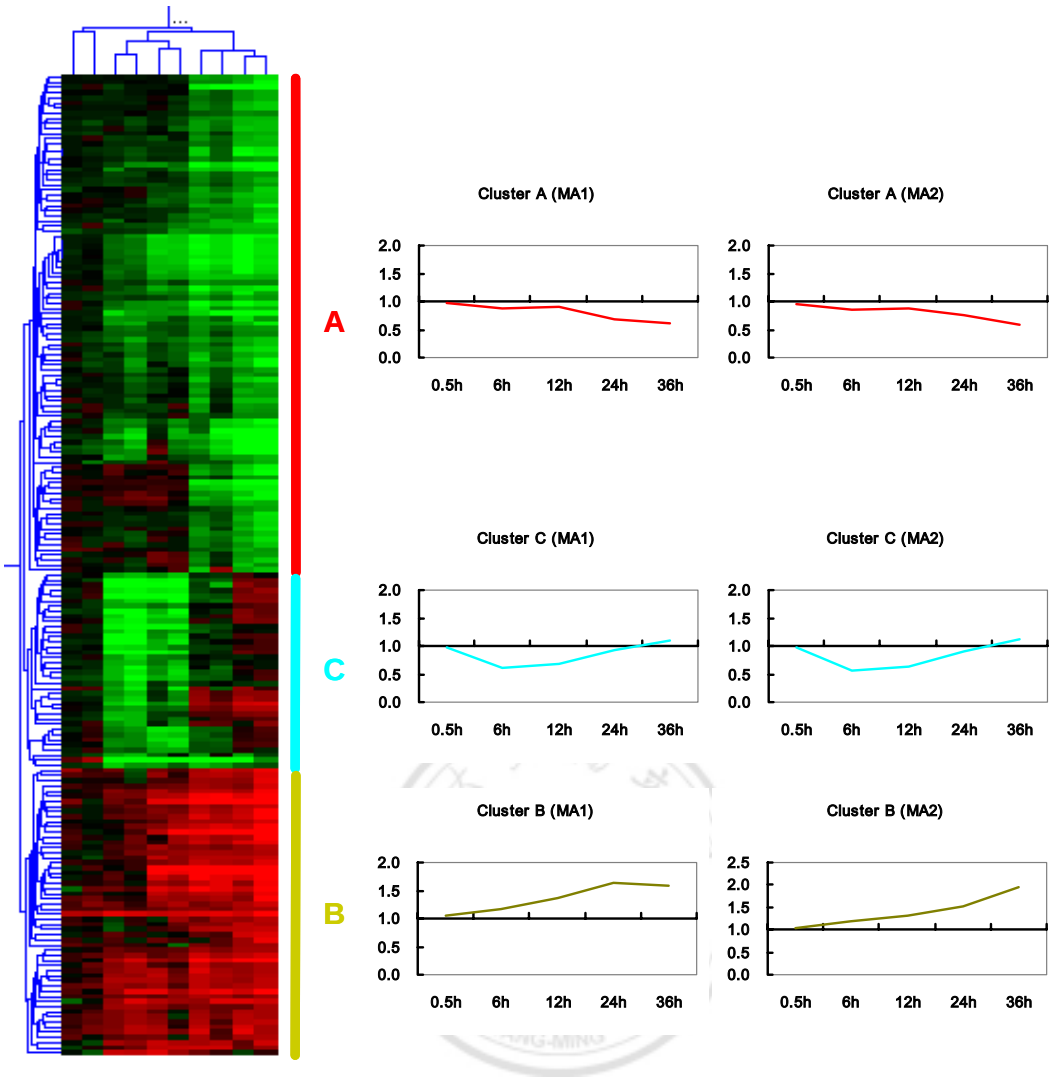

Figure 8. Cluster analysis of gene expression profiles following IR. A total of 196 genes selected for this analysis were clustered into three main groups on the basis of the similarity of their expression profiles. The degree of redness represents level of induction, whereas that of greenness represents level of repression. The black boxes represent genes equally expressed. The charts show the median expression profiles for the genes in the corresponding clusters designated A-C.

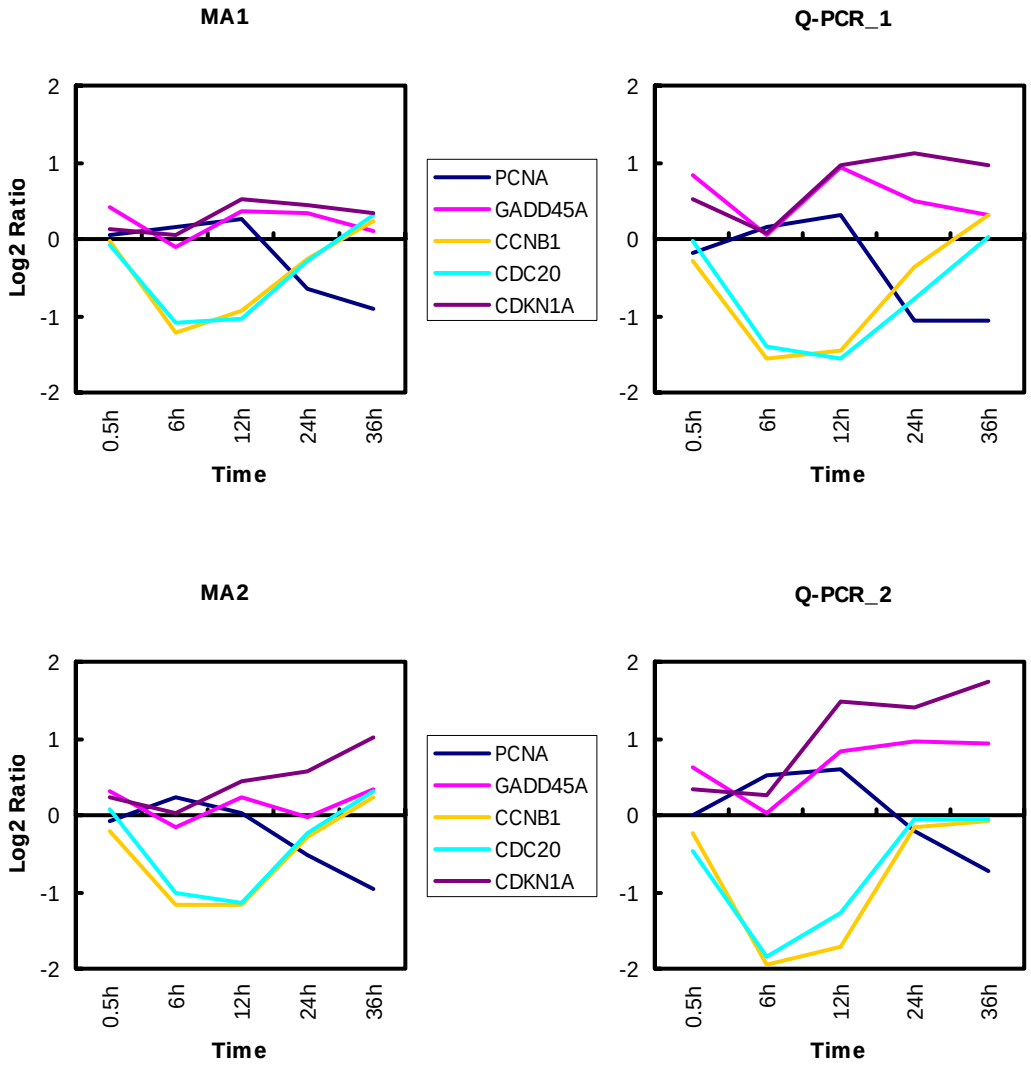

Figure 9. Comparing the results from quantitative RT-PCR and microarray analysis. Independent measurements of selected gene expression levels were performed by quantitative RT-PCR and oligonucleotide microarrays. Expression levels measured by Q-PCR were normalized with GADPH and plotted relative to the level in control cells. Both methods gave similar results in the gene expression profiles.

(A)

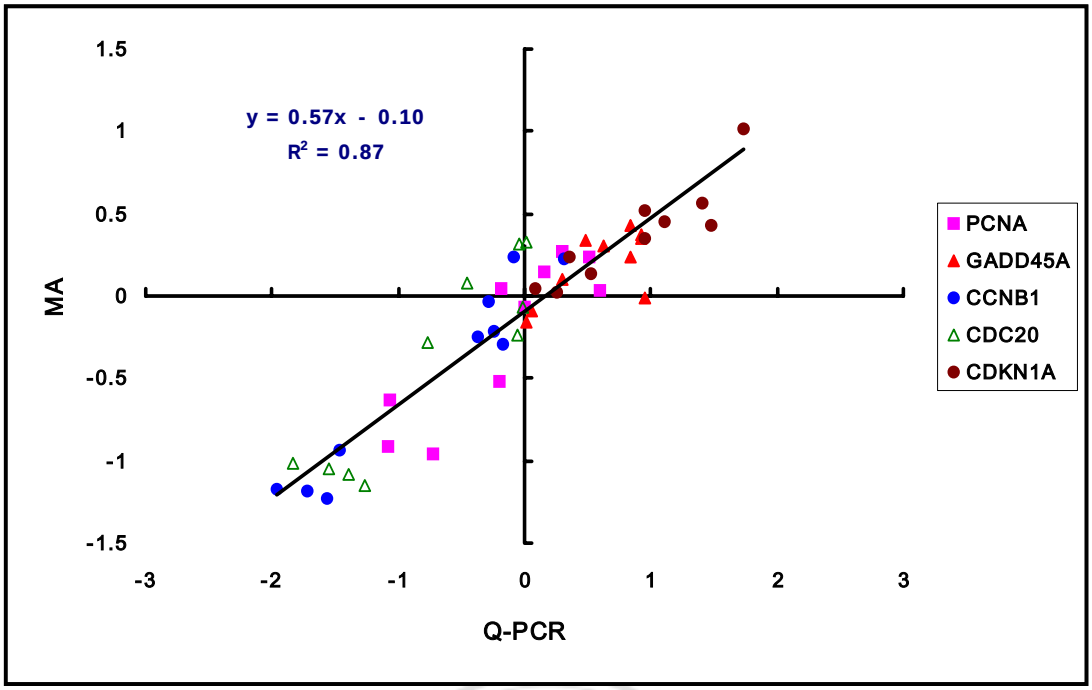

(B)

Q-PCR vs MA	MA1	MA2
PCNA	0.977	0.913
GADD45A	0.898	0.558
CCNB1	0.979	0.926
CDC20	0.938	0.848
CDKN1A	0.914	0.878

Figure 10. Differential gene set validation with quantitative RT-PCR. (A) Five genes, which were identified in microarray analysis, were validated using SYBR Green I assay performed on ABI Prism7000. Results from microarray exhibit high correlation (R^2 = 0.87 for log-transformed expression ratios) with quantitative RT-PCR. (B) The table here shows the Pearson's correlation between Q-PCR and microarary in detailed comparisons.

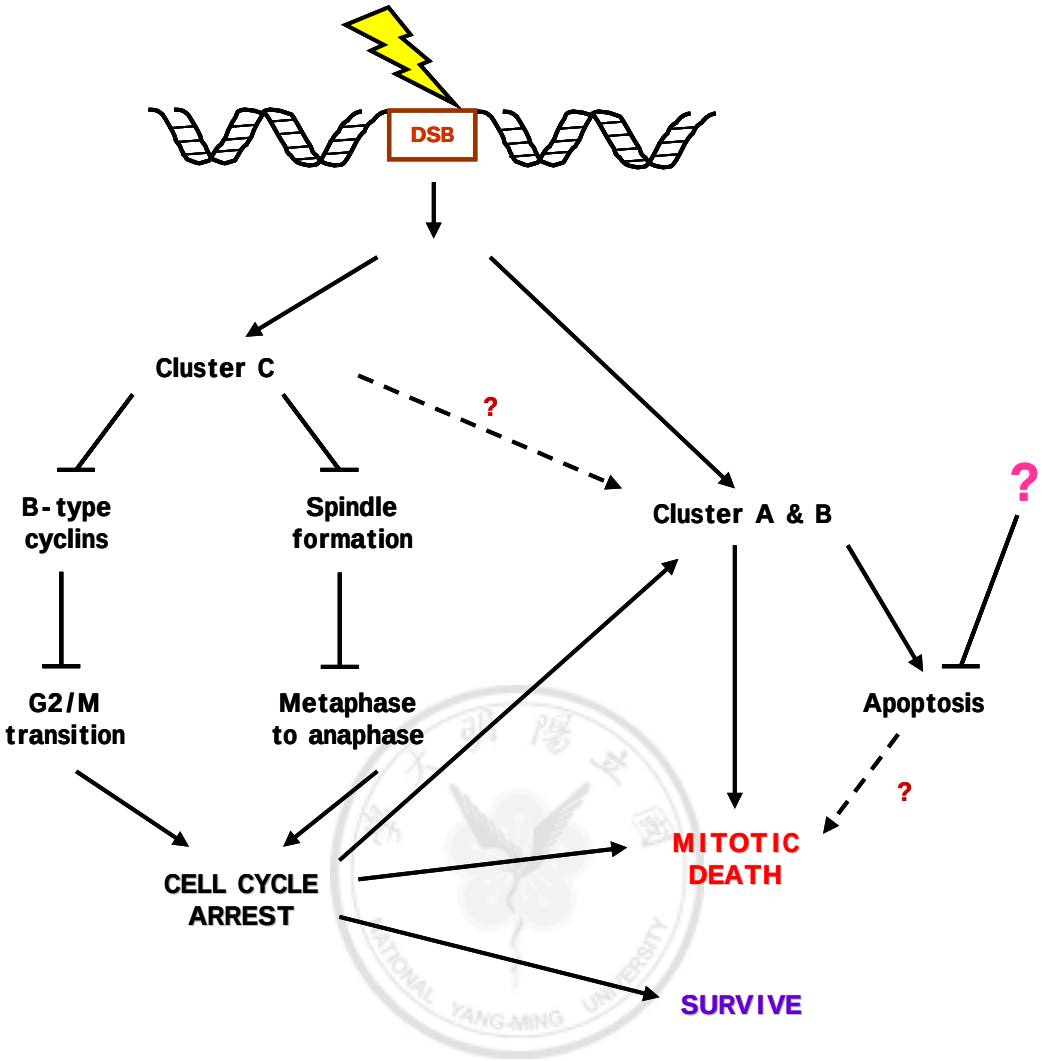

Figure 11. Hypothetical pathway of U138 cells responded to DNA damage. The regulation network in p53-mutant U138 glioma cells after γ-irradiation based on their differential global expression profiles. The radiation-induced transcriptional regulations were activated after detection of DNA double strand breaks (DSB). The genes in cluster C are considered as early responded genes which were suppressed under transcriptional regulations and most of these genes are related to initiate of cell cycle arrest. Then, the genes in cluster A and B were subsequently altered and considered as late responded genes.

APPENDIX: Experiment Protocols

A. Cell culture maintenance

a-1. Cell thawing

1. Heat the water bath to 37^0C, dispense 10 ml medium into a T-75 flask and incubate until cells are to be seeded.
2. Get the sample from the liquid nitrogen tank. Immediately place the vial into the water bath. Avoid submerging the whole vial into the water to avoid contamination.
3. After stock solution has thawed, suck the solution out and dispense slowly into a 10 ml tube.
4. Add medium very slowly to the cell suspension: 10 ml over 2 min added dropwise at the start and then a little faster, gradually diluting the cells and preservatives.(This is particularly important with DMSO, where sudden dilution can cause severe osmotic damage and reduce survival by half.)
5. Centrifuge for 5 min. at 1,000 rpm.
6. Discard the supernatant and flick the tube to suspend the pellet.
7. Add 5 ml of medium and mix. Make sure the solution is homogenous and there are no visible cell pellets.
8. Dispense the solution into the T-75 flask. Observe under the microscope and incubate.
9. After 24 hrs, change half of the medium to remove remaining DMSO.

a-2. Passage of cell line

1. Add medium of appropriate amount to new culture dish/flask to be seeded and incubate.
2. Withdraw the medium and discard.
3. Use 1X PBS as indicated below to rinse the monolayer. Discard the PBS.
4. Add trypsin as indicated below and incubate at 37^0C for 1 to 2 min.

container	1X PBS	Trypsin-EDTA
T-75 flask	2 ml	1.5 ml
T-150 flask	4 ml	2 ml
60 mm dish	2 ml	1 ml
100 mm dish	3 ml	1.5 ml
150 mm dish	4 ml	2 ml

5. Add medium of about two-fold amount of trypsin to stop the reaction of trypsin and disperse the cells by repeated pipeting over the surface bearing the monolayer. Finally, pipette the cell suspension up and down a few times to spread the cells.
6. Transfer the cell suspension to a test tube. Mix and transfer two aliquots into 3 wells of a 96 well plate.
7. Put 80 μl Trypan Blue into 3 wells and add equal amount of cell suspension to make a 1:1 dilution. Mix and load into a hemocytometer and count.
8. Compute for the appropriate volume of cells to be seeded into the new flask or disk. Make sure that the cells are homogenously spread in the new medium. Check under the microscope.
9. Label the passage # and date. Incubate.

B. Growth curve

1. Add 4 ml of fresh medium to each of the forty-five 60mm culture dish and pre-incubate in the 37^0C incubator.
2. Trypsinize the cells (see **Passage of Cell Line**) and centrifuge the cells.
3. Resuspend the pellet in 5 ml of medium and count the cells with hemocounter.
4. Dilute the cell suspension with fresh medium so that the final concentration reaches 1 x 10^4 cells/ml.
5. Add 1 ml of diluted cell suspension to each of the prepared 60mm culture dish.
6. Count some of the leftover cell suspension in order to determine the actual seeding density.
7. Put the plates into the 37^0C incubator supplied with 5% CO_2.
8. Count the triplicate plates every 48 hours.
9. By plotting the results of cell number and time on a log-linear scale, population-doubling time can be determined by identifying a cell number along the exponential phase of the curve.

C. Clonogenic survival assay

Take appropriate number of 100mm dish and seed 3 x 10^5cells per dish. Refresh half medium 24 hrs before irradiation.

1. Prepare enough 60mm culture dishes, label with cell line, passage #, treatment condition, date, seeded cell number. Add 4ml medium per dish and incubate.
2. Cells to be irradiated are sealed with paraffin and irradiate for 0, 2, 4, 6, 8 Gy, respectively.
3. Wash with PBS after irradiation.

4. Trypsinize and count cell numbers with hemocounter. Calculate the concentration and dilute for suitable concentration.
5. Seed cells of appropriate numbers to 60mm dish, incubate at 37^0C for about 10 days.
6. Once the colonies reach appropriate size, stain with 0.5% crystal violet and count the number of cell colony.
7. Calculate survival fraction and plot survival curve.

D. Measurement of DNA content by flow cytometry

1. Collect cells and centrifuge at 1000 rpm for 10 min and remove the supernatant.
2. Transfer cells to a new eppendorf, add 500 μl PBS and pipette gently for washing cells.
3. Centrifuge 2000rpm, 5 min and remove supernatant.
4. Repeat step 2 and 3.
5. Add 70% EtOH (-20^0C) and rock the eppendorf to homogenize.
6. Store at -20^0C at least 30 min, do not over one week.
7. Before performing FCM, centrifuge 7000 rpm, 5min at 4^0C, then remove the supernatant.
8. Add 800 μl PBS, 100 μl RNase A and 100 μl PI, flick and spin down.
9. 37^0C water bath incubate 30 min.
10. Filter by 40μm Nylon membrane and transfer to 12 x 75 mm tube.
11. Seal the tube by paraffin and put on ice.

E. Microarray experiment

e-1. Sample preparation

Cells are seeded at a density of 5 x 10^5 per 100-mm dish in the culture medium for 2 days, and half the medium were refreshed 24 hours prior to 10 Gy irradiation.

1. Cells growing exponentially are irradiated for 10 Gy.
2. For the control sample, go to step 3 without irradiation.
3. Trypsinize and count cell numbers with hemocounter.
4. Wash the cell pellet twice with PBS to remove excess culture medium.
5. Centrifuge at 1000 rpm for 10 min to pellet the cells and completely discard the flow-through.
6. Store at -80^0C for further use.

e-2. Total RNA isolation

1. For pelleted cells, loosen the cell pellet thoroughly by flicking the tube. For cells lesser than 5 x 10^6, add 350 μl of Buffer RLT. Vortex or pipet to mix.
2. Pipet the lysate directly onto a QIAshredder spin column placed in a 2 ml collection tube, and centrifuge for 2 min at maximum speed.
3. Add 350 μl of 70% ethanol to the homogenized lysate, and mix well by pipetting.
4. Apply up to 700 μl of the sample, including any precipitate that might have formed, to an RNeasy mini column placed in a 2 ml collection tube. Centrifuge for 15 sec at 13,000 rpm.
5. Add 700 μl Buffer RW1 to the RNeasy column. Centrifuge for 15 sec at 13,000 rpm. Discard the flow-through and collection tube.
6. Transfer the RNeasy column into a new 2 ml collection tube. Pipet 500 μl Buffer RPE onto the RNeasy column. Centrifuge for 15 sec at 13,000 rpm to wash the column. Discard the flow-through.
7. Add another 500 μl Buffer RPE to the RNeasy column and centrifuge for 2 min at 13,000 rpm to dry the RNeasy silica-gel membrane.
8. To elute, transfer the RNeasy column to a new 1.5 ml collection tube. Pipet 50 μl RNase-free water directly onto the RNeasy silica-gel membrane and stand for 1 min. Centrifuge for for 1 min at 13,000 rpm to elute.
9. Repeat step 8 with 30 μl RNase-free water.
10. Store at -80^{0}C.

e-3. Fluorescent cRNA synthesis and purification

1. To a 1.5 ml microcentrifuge tube, add 2 μg total RNA and 5 μl of T7 Promoter Primer. Use nuclease-free water to bring the total reaction volume to 11.5 μl.
2. Denature the primer and the template by incubating the reaction at 65^{0}C in a heating block for 10 min.
3. Place the reaction on ice and incubate for 5 min.
4. Pre-warm the 5X First Strand Buffer by incubating the vial in a 65^{0}C heating block for 3-4 min.
5. Immediately-prior to use, prepare cDNA Master Mix by gently mixing the following components by pipetting, in the order indicated, at room temperature:

Component	Vol.(μl/rxn)
5X First Strand Buffer	4.0
0.1M DTT	2.0
10 mM dNTP mix	1.0

MMLV RT	1.0
RNase OUT	0.5
Total Volume	8.5

6. To each sample tube, add 8.5 µl cDNA Master Mix. Incubate samples at 40^0C in a circulating water bath for 2 hours.
7. Move samples to a 65^0C heating block and incubate for 15 min and then cooling on ice for 5 min. .
8. Spin samples briefly in a microcentrifuge to drive the tube contents off the tube wall and lid.
9. To each sample tube, add either 2.4 µl cyanine 3-CTP(10mM) or 2.4 µl cyanine 5-CTP(10mM). Be aware to minimize light exposure for the following steps.
10. Pre-warm the 50% PEG solution by incubating the vial in a 40^0C waterbath for 1 min.
11. Immediately-prior to use, prepare the Transcription Master Mix by gently mixing the following components by pipetting, in the order indicated, at room temperature:

Component	Vol.(µl/rxn)
Nuclease-free water	15.3
4X Transcription Buffer	20
0.1M DTT	6.0
NTP mix	8.0
50% PEG	6.4
RNAseOUT	0.5
Inorganic Pyrophosphatase	0.6
T7 RNA Polymerase	0.8
Total Volume	57.6

12. To each sample tube, add 57.6 µl of the Transcription Master Mix. Gently mix by pipetting.
13. Incubate samples in a circulating water bath at 40^0C for 2 hours.

The following steps describe the purification of labeled cRNA samples using Qiagen's RNeasy mini spin column and refrigerated centrifugation procedure by a refrigerated centrifuge set at 4^0C.

14. Add 20 µl of nuclease-free water to the cRNA sample to obtain a total volume of 100 µl.

15. Add 350 μl of Buffer RLT and mix thoroughly.
16. Add 250 μl of ethanol (96-100% purity) and mix thoroughly by pipetting. **DO NOT** centrifuge.
17. Transfer 700 μl of cRNA sample to an RNeasy mini spin column in a 2 ml collection tube. Centrifuge the sample for 30 sec at 13,000 rpm. Discard the flow-through and collection tube.
18. Transfer the RNeasy column to a new collection tube and add 500 μl of Buffer RPE to the column. Centrifuge the sample for 30 sec at 13,000 rpm. Discard the flow-through.
19. Again, add 500 μl of Buffer RPE to the column. Centrifuge the sample for 60 sec at 13,000 rpm. Discard the flow-through and collection tube.
20. Elute the clean cRNA sample by transferring the RNeasy colomn to a new 1.5 ml collection tube. Add 30 μl RNase-free water directly onto the RNeasy filter membrane. Wait 60 sec before centrifuging for 30 sec at 13,000 rpm. **SAVE THE FLOW-THROUGH** and the collection tube.
21. Again, add 30 μl RNase-free water directly onto the RNeasy filter membrane. Wait 60 sec before centrifuging for 30 sec at 13,000 rpm. The total flow through volume should be approximately 60 μl. Store at -80^{0}C until needed.

e-4. Hybridization of oligo microarray

1. Assemble Agilent Microarray Chambers referring to Oligonucleotide Microarray Hybridization Chamber Quick Start Guide for Step-by-step instructions. **Be sure to place the "Agilent" barcode side of the glass slide facing up in the Hybridization chamber.**
2. Prepare 2X Target Solution by mixing the following components by pipetting gently.

0.75 μg cyanine 3-labeled, linearly amplified cRNA
0.75 μg cyanine 5-labeled, linearly amplified cRNA
50 μl 10X Control Targets
Nuclease-free water to volume
Total volume per tube: 250 μl

For each microarray, prepare 1X Hybridization Solution as follows.

3. Add 10 μl 25X Fragmentation Buffer to 250 μl 2X Target Solution.
4. Mix well by gently vortexing. Incubate at 60^{0}C, in a water bath, in the dark, for 30 min.

5. To each tube, add 250μl 2X Hybridization Buffer to terminate the fragmentation reaction, and so the total volume would be 510 μl.
6. Mix well by careful pipetting. Take care to avoid introducing bubbles. Do not vortex: vortexing introduces bubbles.
7. Spin briefly in a microcentrifuge to drive the sample to the bottom of the tube.
8. Use immediately. Do not store.
9. For each microarray, insert a 25-gauge needle into the opening of one of the septa installed in the chamber.
10. Fit a 1 ml syringe with a second needle.
11. Slowly draw up the entire amount of solution from one tube, avoiding any bubbles in the solution.
12. Spin the sample tube again briefly in a microcentrifuge to consolidate any remaining sample in the tube bottom. Slowly draw up any remaining sample into the 1 ml syringe avoiding bubbles.
13. Slowly inject the solution into the septa that doesn't have the needle in it. Completely fill the chamber with the hybridization solution.
14. Remove the needles from the septa. Discard the needles in an appropriate waste container.
15. If bubbles did form during loading, verify that they rotate freely in the hybridization chamber by viewing the solution from the back while slowly rotating the chamber.
16. Place the hybridization chamber on the hybridization rotator rack in the hybridization oven, at 60^0C. Each hybridization chamber is clamped on its side and is rotated end-over-end on the hybridization rotator.
17. Proceed with other slides by adding the hybridization solution, as described above.
18. Hybridize at 60^0C, in the dark, for 17 hours.

e-5. Wash of slides and scanning

Before the incubation has finished, prepare three staining dishes as followed:

- To the first staining dish (large volume, approximate 250 ml, to facilitate disassembly of hybridization chambers), add **Wash Solution 1** containing 6X SSC and 0.005% Triton X-102, at room temperature.
- To the second staining dish, add a slide rack and a magnetic stir bar, Cover the rack with room temperature Wash Solution 1. Place the dish on a magnetic stir plate.
- Place the third staining dish into another container filled with ice (a Pyrex loaf pan is well-suited to this purpose). Add a Magnetic stir bar. Add 4^0C **Wash**

Solution 2 containing 0.1X SSC and 0.005% Triton X-102 to a depth sufficient to cover a slide rack. Be sure to replenish the ice in the outer container, which will keep the solution as cold as possible.

1. Remove only one hybridization chamber from the oven at a time to avoid chamber cool-down before disassembly in the wash dish.
2. Immerse one chamber in the first staining dish, filled with **Wash Solution 1.**
3. Disassemble the chamber quickly, while immersed, by sequentially unscrewing the tops from the hybridization chamber. This step should be completed promptly, without interruptions.
4. Remove the glass slide and quickly place it in the slide rack in the second staining dish, containing **Wash Solution 1** at room temperature. Be careful to touch only the barcoded portion of the slide or its edges.
5. Repeat step 1-4 for the other slides.
6. After all slides have been collected in the slide rack, set the magnetic stir plate to a medium speed. Wash slides for 10 min at room temperature.
7. Transfer the slide rack to the third staining dish containing **Wash Solution 2,** which is on ice. Place the entire dish on a magnetic stirring plate set to medium speed. Wash slides for 5 min.
8. The slide rack containing slides must stay immersed in the **Wash Solution 2** during the individual slide drying process. Dry each slide, one slide at a time. Remove one slide from the slide rack. Using a nitrogen-filled air gun, quickly blow drops of solution from the slide surface. Repeat procedure for each individual slide in the slide rack.
9. To measure fluorescence intensities, load slides into a microarray scanner.
10. After scanning, store slides in polypropylene slide boxes, in a vacuum desiccator or a nitrogen purge box, in the dark.

F. Real-time RT-PCR

f-1. Reverse transcription

(The following protocol is for 1μg total RNA as starting materials. Multiply the volume of reagents accordingly.)

1. Preparing the following mixture so that the total volume is 12 μl, on ice.

total RNA	(1 μg)
oligo$(dT)_{12\text{-}18}$	1 μl
10mM dNTP mix	1 μl

RNase-free water	to volume
total volume	12 μl

2. Heat the mixture to 65^0C for 5 mins and quickly chill on ice
3. Add the following to the mixture.

5X first-strand buffer	4 μl
0.1M DTT	2 μl
RNaseOUT Recombinant Ribonuclease Inhibitor(40 units/μl)	1 μl

4. Mix the content gently and incubate at 42^0C for 2 min.
5. Add 1 μl (200 units) of SuperScriptII RT.
6. Incubate at 42^0C for 50 min.
7. Inactivate the reaction by heating at 70^0C for 15 min.
8. Store the cDNA at -20^0C for further use.

f-2. cDNA purification

1. Add 5 volumes of Buffer PB to 1 volume of the cDNA sample and mix.
2. Place a QIAquick spin column in a 2 ml collection tube.
3. To bind DNA, apply the sample to QIAquick column and centrifuge for 60 sec.
4. Discard flow-through and centrifuge the column for an additional 1 min.
5. Place the QIAquick column in a new 1.5 ml tube.
6. To elute DNA, add 50 μl Buffer EB or H_2O to the QIAquick membrane, let stands for 1 min, and centrifuge the column for 1 min.
7. Store at -20^0C.

f-3. Real-time Polymerase Chain Reaction

1. Normalize the primer concentrations and mix gene-specific forward and reverse primer pair. Each primer (forward or reverse) concentration in the mixture is 1 μM.
2. The total volume of a real-time PCR reaction mixture for each well is 30 μl containing 20 ng cDNA. Prepare the following mixture in a 1.5ml tube for triplicates.

cDNA	20 ng

primer pair mix (1μM/each primer)	18 μl
distilled water	to volume
2X SYBR Green Master Mix	45 μl
total volume	90 μl

3. Load the samples as triplicates into 96-well PCR plate.
4. Set up the experiment and the following PCR program on ABI Prism 7000 and do remember to click on the dissociation protocol at 60^0C:

   Step1. 50^0C 2 min, 1 cycle

   Step2. 95^0C 10 min, 1 cycle

   Step3. 95^0C 15 sec then 60^0C 1 min, 40 cycles
5. After PCR is finished, analyze the real-time PCR result with the ABI Prism 7000 SDS software. Check to make sure there is neither bimodal dissociation curve nor abnormal amplification plot.

Experimental Flowchart

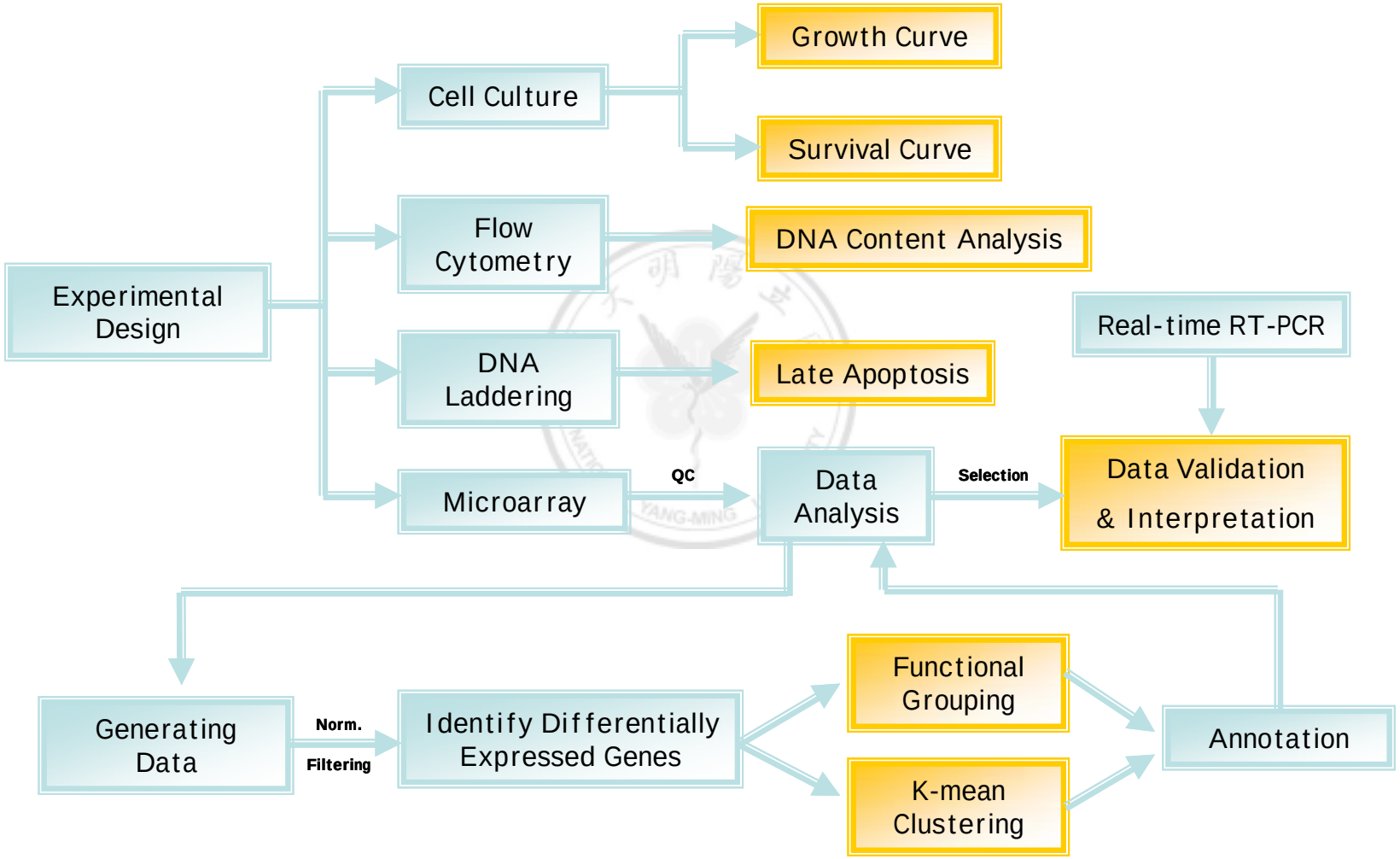

Microarray Experimental Design

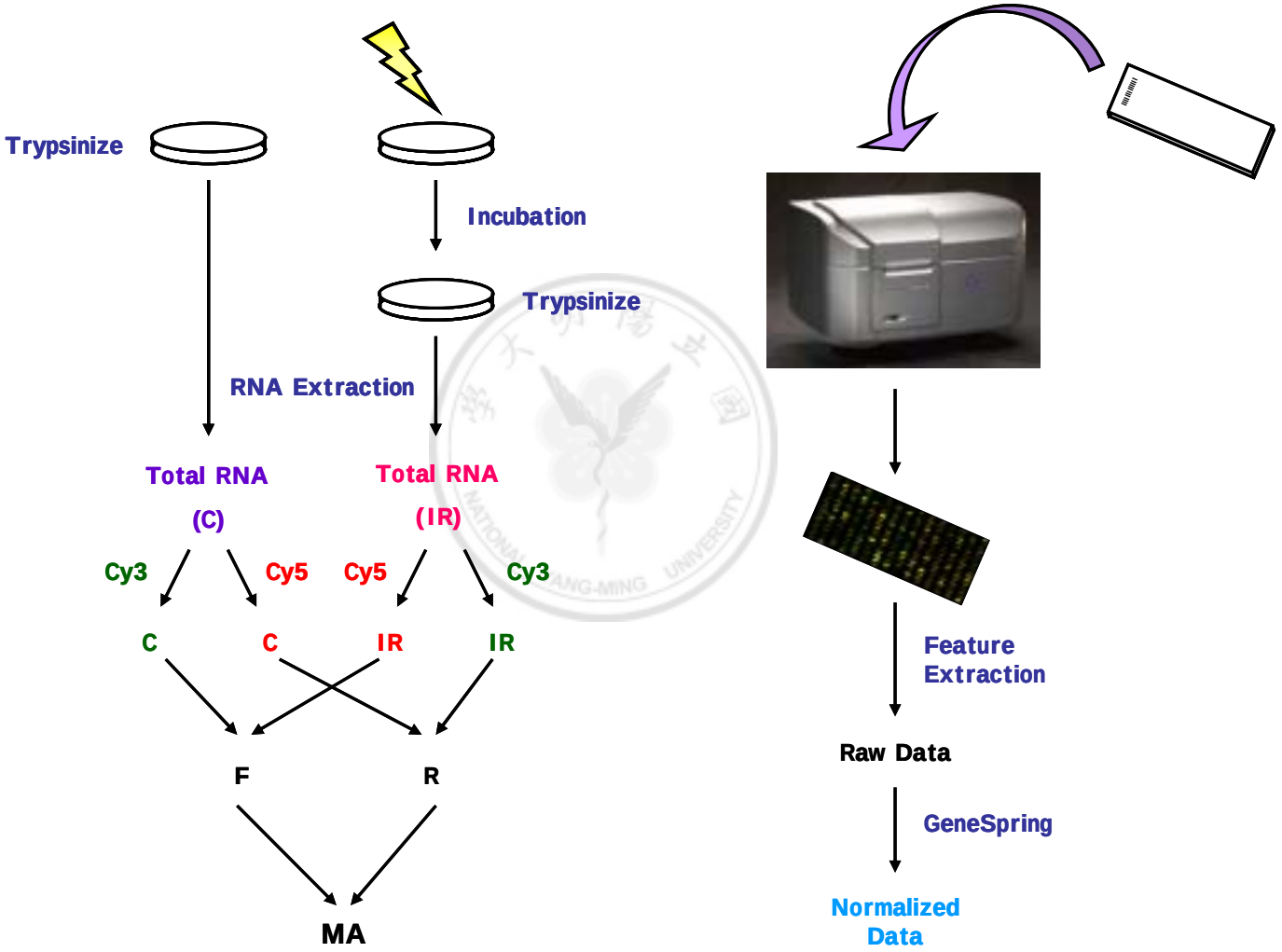

NATIONAL YANG-MING UNIVERSITY